Tectonophysics 602 (2013) 124–140

Contents lists available at SciVerse ScienceDirect

Tectonophysics

journal homepage: www.elsevier.com/locate/tecto

Slab detachment during continental collision: Influence of crustal rheology and interaction with lithospheric delamination

T. Duretz [a,b,*], T.V. Gerya [b]

[a] ISTEP, UMR 7193, UPMC Paris 06, CNRS, Paris, France
[b] Institute of Geophysics, Department of Earth Sciences, ETH Zürich, Sonnegstrasse 5, 8092 Zurich, Switzerland

ARTICLE INFO

Article history:
Received 22 December 2011
Received in revised form 30 November 2012
Accepted 23 December 2012
Available online 14 January 2013

Keywords:
Topography
Crust rheology
Continental collision
Slab detachment
Slab retreat

ABSTRACT

Collision between continents can lead to the subduction of continental material. If the crust remains coupled to the downgoing slab, a large buoyancy force is generated. This force slows down convergence and promotes slab detachment. If the crust resists to subduction, it may decouple from the downgoing slab and be subjected to buoyant extrusion.

We employ two-dimensional thermo-mechanical modelling to study the importance of crustal rheology on the evolution of subduction–collision systems. We propose simple quantifications of the mechanical decoupling between lithospheric levels (σ^*) and the potential for buoyant extrusion of the crust (ξ^*). The modelling results indicate that a variable crustal rheological structure results in slab detachment, delamination, or the combination of both mechanisms.

A strong crust provides coupling at the Moho (low σ^*) and remains coherent during subduction (low ξ). It promotes deep subduction of the crust (180 km) and slab detachment. Exhumation occurs in coherent manners via eduction and thrusting. Slab detachment triggers the development of topography (>4.5 km) close to the suture. A contrasting style of collision occurs using a weak crustal rheology. Mechanical decoupling at the Moho (high σ^*) promotes the extrusion of the crust (high ξ), disabling slab detachment. Ongoing shortening leads to buckling of the crust and development of topography on the lower plate. Collisions involving rheologically layered crust allow decoupling at mid-crustal depths. This structure favours both the extrusion of upper crust and the subduction of the lower crust. Such collisions are successively affected by delamination and slab detachment. Topography develops together with the buoyant extrusion of crust onto the foreland and is further amplified by slab detachment.

Our results suggest that the occurrence of both delamination (Apennines) and slab detachment (Himalayas) in orogens may indicate differences in the initial crustal structure of subducting continental plates in these regions.

1. Introduction

The slab detachment (or slab breakoff) model has been widely employed in the interpretation of both geological and geophysical observation. This model involves the detachment of a portion or the integrity of a subducting slab beneath a convergent margin. The concept of slab detachment was born from seismological studies and was first hypothesised in the late sixties (Isacks and Molnar, 1969) in order to explain seismicity patterns in subduction zones. The study of deep seismicity patterns has indicated the existence of seismogenic zones that were associated to gaps within slabs (Chatelain et al., 1993; Chen and Brudzinski, 2001; Kundu and Gahalaut, 2011; Sperner et al., 2001). The slab detachment model has further gained popularity with the development of seismic tomography (Levin et al., 2002; Rogers et al., 2002; Schmandt and Humphreys, 2011; van der Meer et al., 2010; Widiyantoro and van der Hilst, 1996; Wortel and Spakman, 1992; Zor, 2008). Moreover, regional scale seismic tomography has enabled the detection of positive seismic velocity anomalies beneath collision zones, these structures were consequently attributed to detached or detaching slab (Lippitsch et al., 2003; Martin and Wenzel, 2006; Replumaz et al., 2010; Wortel and Spakman, 2000).

Slab detachment is likely to take place once large tensional stresses develop within the down-going slab. Slowdown of the subduction rate is a plausible mechanism that accounts for tensional stress build up as long as the slab pull force is constant (Li and Liao, 2002), such situation may take place following the subduction of an attempted ridge (Andrews and Billen, 2009; Burkett and Billen, 2011) or during the subduction of continental material (Baumann et al., 2009; Duretz et al., 2011; van Hunen and Allen, 2011). The slab detachment model is likely to be a fast geological process (Duretz et al., 2012b) leading to (1) a partial or complete loss of the slab pull force and (2) the inflow of hot asthenosphere at the location of the detachment. The loss of slab pull

* Corresponding author at: Institute of Geophysics, Department of Earth Sciences, ETH Zürich, Sonnegstrasse 5, 8092 Zurich, Switzerland. Tel.: +33 1 44 27 59 07.
E-mail address: Thibault.Duretz@erdw.ethz.ch (T. Duretz).

0040-1951/$ – see front matter © 2013 Elsevier B.V. All rights reserved.
http://dx.doi.org/10.1016/j.tecto.2012.12.024

leads to force rebalancing in the orogen which can potentially triggers a wide range of dynamical effects. The slab detachment model was consequently used for the explanation of high pressure and ultra-high pressure rock exhumation (Andersen et al., 1991; Babist et al., 2006; Xu et al., 2010), variations in surface uplift rates (Morley and Back, 2008; Rogers et al., 2002; Wilmsen et al., 2009) and in the sedimentary record (Mugnier and Huyghe, 2006; Sinclair, 1997), orogenic extension (Zeck, 1996), rapid changes in plate motions (Austermann et al., 2011), or reversal of the subduction dip (Regard et al., 2008). The inflow of asthenosphere within a detaching slab is usually considered as an efficient mechanism to advect heat at lithospheric to sub crustal level (van de Zedde and Wortel, 2001) potentially leading to partial melting in the mantle (Altunkaynak and Can Genç, 2004; Davies and von Blanckenburg, 1995; Ferrari, 2004) in association to plutonism and volcanism (Ferrari, 2004; Keskin, 2003; Qin et al., 2008).

A number of analytical, analogue and numerical modelling studies have focussed on slab detachment (Andrews and Billen, 2009; Baumann et al., 2009; Buiter et al., 2002; Burkett and Billen, 2011; Cloetingh et al., 2004; Davies and von Blanckenburg, 1995; Duretz et al., 2011; Gerya et al., 2004; Li and Liao, 2002; Macera et al., 2008; Regard et al., 2008; Schmalholz, 2011; Ton and Wortel, 1997; Toussaint et al., 2004; van de Zedde and Wortel, 2001; van Hunen and Allen, 2011). These studies were designed to evaluate the depth slab detachment (Baumann et al., 2009; Duretz et al., 2011; Gerya et al., 2004; van de Zedde and Wortel, 2001), its duration (Andrews and Billen, 2009; Baumann et al., 2009; Duretz et al., 2012b; Gerya et al., 2004), and its topographic expression (Buiter et al., 2002; Duretz et al., 2011; Gerya et al., 2004), as well as the dynamic consequences of slab pull loss (Duretz et al., 2012a). Recently, three dimensional aspects of slab detachment have been addressed in numerical experiments. These simulations (Burkett and Billen, 2011; van Hunen and Allen, 2011) have highlighted the role of slab rheology and margin obliquity on the style of detachment (tear versus boudinage). The studies of Andrews and Billen (2009) and Schmalholz (2011) have further stressed the importance of a non-Newtonian rheology for slabs to undergo lithospheric-scale boudinage, ultimately leading to detachment.

Slab detachment in a collisional context is likely to take place within the subducting continental margin (Baumann et al., 2009; Gerya et al., 2004; van Hunen and Allen, 2011). It can thus be expected that crustal rheology, which controls the mechanical coupling at the Moho (Le Pourhiet et al., 2006; Nakada, 1994; Toussaint et al., 2004), plays an important role in the occurrence of slab detachment. Moreover, one may expect that changing the rheological structure of the crust may control the occurrence of other orogenic processes such as lithospheric delamination (Bird, 1979). Despite that fact, the role of crustal rheology on the occurrence of slab detachment has not yet been investigated. We therefore use two-dimensional thermo-mechanical modelling to study the influence of continental crust rheology on the occurrence of slab detachment, collision dynamics and topographic evolution of subduction/collision zones.

2. Modelling approach

2.1. Methodology

In order to simulate the dynamics of upper mantle scale processes coupled to topographic development, we employ the thermo-mechanical code I2VIS (Gerya, 2010; Gerya and Yuen, 2003a). This numerical code solves for the two-dimensional steady state momentum equations and heat conservation equation using the finite-difference/marker-in-cell method on a Eulerian grid (Gerya, 2010; Gerya and Yuen, 2003a):

$$\frac{\partial \sigma_{ij}}{\partial x_j} - \frac{\partial p}{\partial x_i} = -\rho g_i \tag{1}$$

$$\frac{\partial v_i}{\partial x_i} = 0 \tag{2}$$

$$\frac{\partial}{\partial x_i}\left(k\frac{\partial T}{\partial x_i}\right) = \rho C_p \frac{DT}{Dt} - H \tag{3}$$

where x_j represents the coordinates, ρ, the material density (kg/m^3), k, the thermal conductivity (W/m/K), C_p, the isobaric heat capacity (J/kg) and H (J/m^3/s), the contribution of internal heat sources (radiogenic, shear, and adiabatic heating).

The mechanical model employs a velocity formulation and the deviatoric stress tensor σ_{ij} relates to the material viscosity η_{eff} and the rate of deformation tensor $\dot{\epsilon}_{ij}$ via:

$$\sigma_{ij} = 2\eta_{\text{eff}}\dot{\epsilon}_{ij} = \eta_{\text{eff}}\left(\frac{\partial v_i}{\partial x_j} + \frac{\partial v_j}{\partial x_i}\right) \tag{4}$$

All the lithologies deform according to a visco-plastic rheological model. This model combines the contribution of Newtonian and non-Newtoninan flow rules that control the effective viscosity of each material phase. A more detailed description of this rheological model is given in Section 1.

The model's surface h (air/crust interface) evolves following a gross-scale erosion–sedimentation law (Gerya, 2010; Gerya and Yuen, 2003b):

$$\frac{\partial h}{\partial t} = v_y - v_x\frac{\partial h}{\partial x} - \dot{e} + \dot{s} \tag{5}$$

where v_y and v_x are the uplift and advection velocity (m/s) predicted by the tectonic model, $\dot{e}$ and $\dot{s}$ represent prescribed erosion and sedimentation rates ($\dot{e} = 0.1$ mm/yr if $h > 1$ km and $\dot{s} = 0.1$ mm/yr if $h < -1$ km).

The Lagrangian advection equation is solved by an explicit coordinate update of the markers that carry the material properties through the Eulerian grid.

The density and heat capacity of each lithology are pressure P (Pa) and temperature T (K) dependent and are updated at each timestep. We assume a pyrolitic mantle composition and a basaltic–gabbroic oceanic crust. Their properties are pre-computed using Gibbs free energy minimisation with the chemical model CaO–FeO–MgO–Al_2O_3–SiO_2 (Baumann et al., 2009; Gerya et al., 2004). The density of felsic materials are obtained from the equation of state:

$$\rho = \rho_0\left(1-\alpha(T-298.15)\right)\left(1+\beta\left(P\times 10^{-8}-10^{-3}\right)\right), \tag{6}$$

where ρ_0 corresponds to the reference density (2700 kg/m^3 for the upper crust and 2800 kg/m^3 for the lower crust), β to the isothermal compressibility (0.5×10^{-3} kbar^{-1}) and α to the thermal expansivity (1.5×10^{-5} K^{-1}). The thermal conductivity k is a function of the temperature (Clauser and Huenges, 1995), the functions used to evaluate k are listed in Table 1. The presented simulations do not take into account the effects of partial melting and hydration/dehydration processes.

2.2. Setup

The model domain consists initially of two continental plates separated by an oceanic basin (Fig. 1). The dimensions of the model box is 4000×1400 km^2 (1361×351 nodes), all the mechanical boundaries are free slip. Variable grid spacing enables to reach a 1 km grid resolution in the central part of the domain where the continental collision takes place. In order to study the interplay between subduction and orogenic evolution, we follow the semi dynamic approach employed in Baumann et al. (2009) and Duretz et al. (2011). The initial conditions of the model are built during a stage of kinematic

Table 1
List of thermal and plastic (Mohr–Coulomb) parameters fused in the simulations, H_r is the radiogenic heat production, C_p is the specific heat capacity, ϕ is the internal friction angle, and C is the cohesion.

Material	k (W/m/K)	H_r (W/m^3)	Cp (J/kg)	sin(ϕ)	C (MPa)
Sediments	$0.64+\frac{807}{T+77}$	1.5×10^{-6}	1000	0.15	1
Upper cont. crust	$0.64+\frac{807}{T+77}$	1.00×10^{-6}	1000	0.15	1
Lower cont. crust	$1.18+\frac{474}{T+77}$	0.25×10^{-6}	1000	0.15	1
Upper oceanic crust	$0.64+\frac{807}{T+77}$	0.25×10^{-6}	1000	0.00	1
Lower oceanic crust	$1.18+\frac{474}{T+77}$	0.25×10^{-6}	1000	0.60	1
Mantle	$0.73+\frac{1293}{T+77}$	2.20×10^{-8}	1000	0.60	1
Weak zone	$0.73+\frac{1293}{T+77}$	2.20×10^{-8}	1000	0.00	1

convergence. During this period, the oceanic subduction is kinematically prescribed using internal kinematic constrains (1.25 cm/yr until 500 km of convergence is accommodated). With ongoing convergence, the two converging plates decouple from the lateral sides of the box, these zones accommodate hot mantle upwellings and are therefore the location where oceanic ridges spontaneously develop (Fig. 1). At the end of this period of forced convergence, the obtained thermo-mechanical state is employed as the initial condition for continental collision. After this model initialisation step, the internal kinematic constrain is removed and the model is driven by internal forces. The collision rates, which are not in steady state, are controlled by the contribution of slab pull, crustal buoyancy, ridge pushes (from both sides), and dissipative forces. In our models, the dominant forces are represented by both the slab pull and the crustal buoyancy (Duretz et al., 2012a). We employ an additional 20 km thick layer of sticky air ($\eta_{air}=10^{18}$ Pa.s, $\rho_{air}=1$ kg/m^3) in order to mimic the effect of a free surface and enable the development of topography (Crameri et al., 2012; Schmeling et al., 2008). The initial slab temperature field is defined using the half-space cooling model (Turcotte and Schubert, 1982) using a slab age of 40 Ma and a diffusivity of 10^{-6} m^2.s^{-1}. The initial continental geotherm is defined as a linear temperature variation from the model surface (T = 293 K) to the lithosphere–asthenosphere boundary (T = 1617.6 K), the left and right sides of the model domain are insulating boundaries.

3. Strength of the lithospheric model

3.1. Rheological model

We consider that the strength of the lithosphere is controlled, at the timescale of orogeny, by the combination of both brittle and ductile deformation mechanisms. The brittle part of the lithosphere is controlled by Mohr–Coulomb (or Drucker–Prager) plasticity which expresses the linear dependence of the geomaterials resistance on the total pressure. Mohr–Coulomb plasticity acts as a stress limiter in the regions where the second stress invariant (σ_{II}) exceeds the material yield stress. The yield stress depends on the pressure, the standard strength C (MPa), and the internal friction angle ϕ. The stress is limited via local effective viscosity (η_{eff}) reduction such that

$$\eta_{eff} \leq \frac{C + Psin(\phi)}{2\sqrt{\dot{\epsilon}_{II}}} \tag{7}$$

Our rheological model takes into account a second semi-brittle deformation mechanism characterised by the exponential flow of olivine (or Peierls mechanism). This flow mechanism has been put in evidence in a number experimental studies (Evans and Goetze, 1979; Katayama and Karato, 2008; Mei et al., 2011; Raterron et al., 2004). Katayama and Karato (2008) have shown that Peierls creep is likely to be activated in the thermo-mechanical conditions of subduction. Moreover, recent studies have shown that the existence of plate tectonics requires sufficiently lithospheric yield stress that are lower than Mohr–Coulomb stresses (vam Heck and Tackley, 2008). Such conditions necessitate the use of stress limiters such as Peierls creep which promotes the localisation of deformation in the lithospheric mantle (Kameyama et al., 1999; Lu et al., 2011). In a collisional context, this Peierls creep was shown to have a strong influence on slab detachment's depth and timing (Duretz et al., 2011). The effective viscosity corresponding to the Peierls creep regime is characterised by an exponential dependance on the second stress invariant and is formulated as:

$$\eta_{Peierls} = \frac{1}{2A_{Peierls}\sigma_{II}\, exp\left[\left(\frac{E_a - PV_a}{RT}\right)\left(1-\left(\frac{\sigma_{II}}{\sigma_{Peierls}}\right)^k\right)^q\right]} \tag{8}$$

E_a corresponds to the activation energy (J/mol), V_a is the activation volume (J/bar/mol) and R is the gas constant (8.314472 J/mol/K). We employ the dry olivine parameters $A_{Peierls}=10^{7.8}\times10^{-12}$ Pa^{-2} s^{-1} and $\sigma_{Peierls}=9.1$ GPa (Evans and Goetze, 1979). The activation of Peierls creep is allowed for temperatures lower than 1373 K.

Diffusion–dislocation creep of rocks is temperature, pressure and stress-dependent. Both mechanisms are taken into account by defining an effective viscous rheology. Such composite rheology is implemented

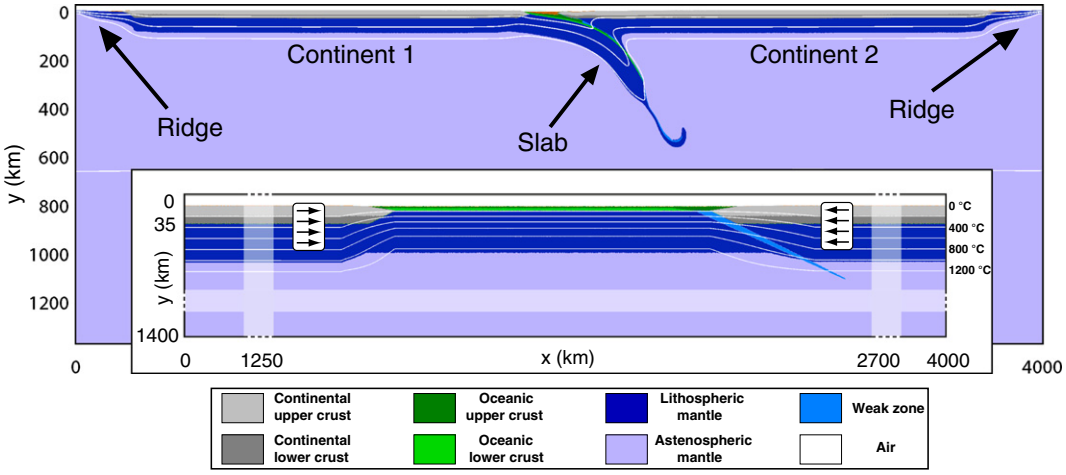

Fig. 1. Initial phase distribution in the model domain (cropped area) and evolved simulation (after 38 Myr of convergence). The slab temperature is computed according to a half-space cooling model given an age of 40 Myr. The continental geotherms are both initially linear. A symmetric total convergence rate of 1.25 cm/yr is imposed at the location of the arrows until 500 km of convergence has been reached. The shaded areas and dashed lines represent breaks in the model's scale.

as the sum of the diffusion ($\dot{\epsilon}_{diff}$) and dislocation ($\dot{\epsilon}_{dis}$) creep strain rates:

$$\dot{\epsilon} = \dot{\epsilon}_{diff} + \dot{\epsilon}_{dis} \quad (9)$$

Both mechanisms are active at each lithospheric level as long as the current state of stress (σ_{II}) does not exceed either Mohr–Coulomb or Peierls stress limiters. At stresses larger than 30 kPa, most of the flow occurs in the dislocation creep regime (Turcotte and Schubert, 1982) and depends non-linearly on the second invariant of the strain rate tensor ($\dot{\epsilon}_{II}$). The effective viscosity corresponding to a diffusion–dislocation creep regime is calculated as following:

$$\eta_{creep} = \eta_0^{\frac{1}{n}} \dot{\epsilon}_{II}^{\frac{1-n}{2n}} \exp\left(\frac{E_a + PV_a}{nRT}\right) \quad (10)$$

where n is the stress exponent (with n = 1 for diffusion creep) and η_0 is the reference viscosity (Pa ^{n}.s). In practical, the effective viscosity corresponding to each flow rule (Mohr–Coulomb, Peierls, diffusion–dislocation) is calculated for each lithology. The mechanism that produces the lowest stress is defined as the active deformation mechanism. For practical reasons, the effective viscosity is limited such as $10^{18} < \eta < 10^{25}$ Pa.s.

3.2. Lithospheric rheological models

The first order contribution of rheological model to the lithospheric strength can be probed by the use of rheological profiles or "Christmas trees" (Afonso and Ranalli, 2004; Burov and Watts, 2006; Jackson, 2002; Ranalli, 1995). Although this representation usually assume a constant average strain rate ($\dot{\epsilon}_{av}$) through the entire lithospheric column (upper/lower crust (UC/LC), mantle lithosphere (ML)), they can be used as first order indicators of the lithospheric strength (F) for modelling purposes (Gerbault and Willingshofer, 2004; Mareschal, 1994; Schmalholz et al., 2009; Thompson et al., 2001; Toussaint et al., 2004). We define three main end-members that are characterised by the rheology of the continental crust (Fig. 2). The stress profiles a generated for a crustal thickness of 35 km, a Moho temperature of 450 C and a lithostatic pressure gradient. This set of parameters reflects the pre-collisional state of stress in our simulations, which will evolve during convergence and collision according to stress, temperature and pressure. Each lithospheric end-member contains a strong upper mantle rheology that can account for the coherent development of subduction and the long-term support of topography (Burov, 2011; Burov and Watts, 2006). The rheological parameters that are employed to calculate the different rheological profiles are listed in Tables 1 and 2. We define weak and a strong rheological profiles that correspond to crustal rheologies that are either dominated by quartz or felspar (Ranalli,

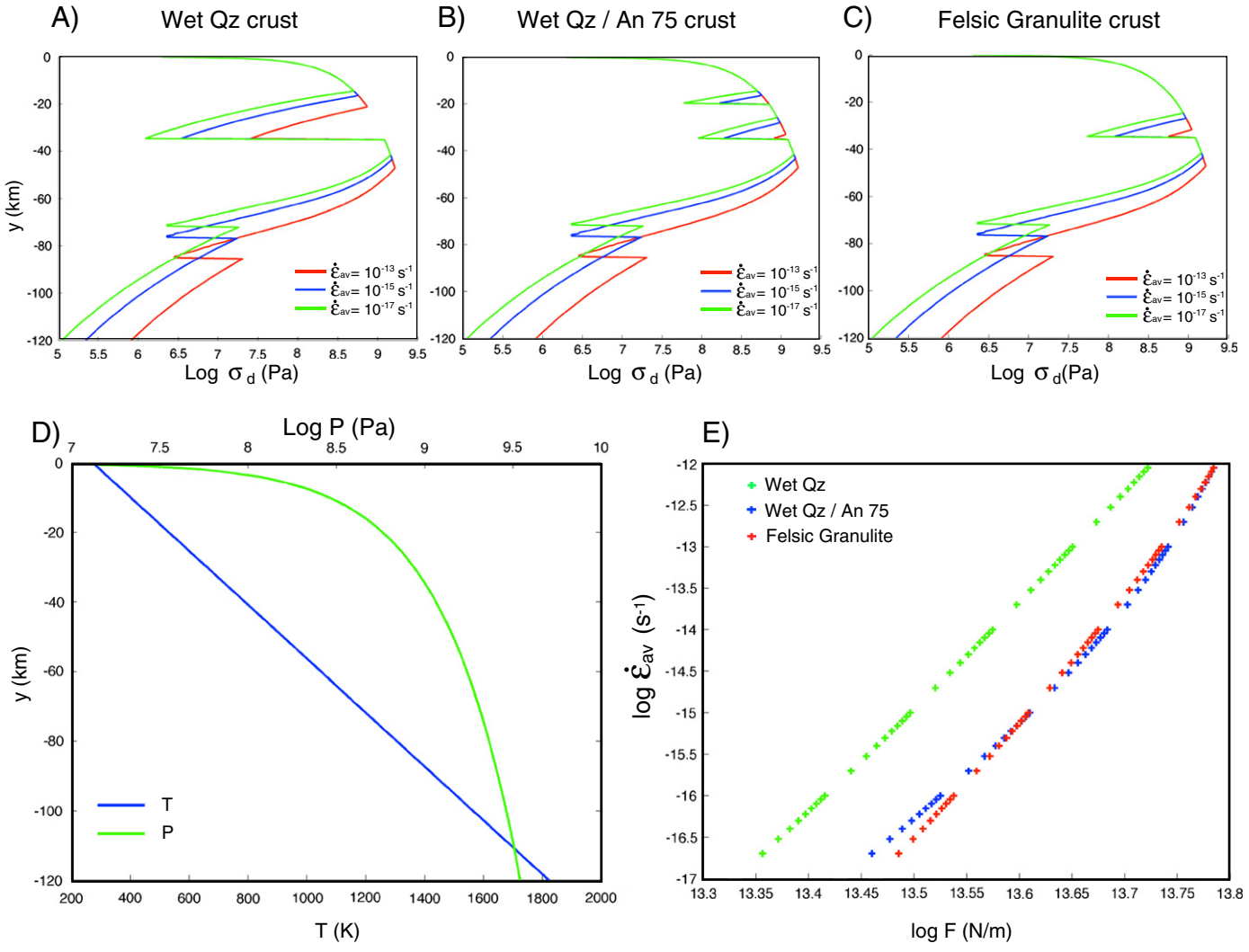

Fig. 2. Example of rheological profiles for the different strength end-members for 3 different average strain rates. A) Weak crust: quartzite rheology. B) Layered quartzite/feldspar crust. C) Felsic granulite crust. D) Corresponding pressure and temperature profiles. E) Integrated strength versus average strain rate diagram for the three different lithosphere models.

Table 2
Ductile creep parameters corresponding to the different rheologies employed in the simulations, η_0 is the reference viscosity, n is the stress exponent, E_a is the activation energy, and V_a is the activation volume.

Flow law	η_0 ($Pa^n s$)	n	E_a (J/mol)	V_a (J/bar/mol)
Wet quartzite	1.97×10^{17}	2.3	1.54×10^{5}	0.8
Plagioclase (An75)	4.80×10^{22}	3.2	2.38×10^{5}	1.2
Felsic granulite	4.97×10^{20}	3.1	2.43×10^{5}	1.2
Dry olivine	3.98×10^{16}	3.5	5.32×10^{5}	0.8
Wet olivine	5.01×10^{20}	4.0	4.70×10^{5}	0.8

2000). The single layered quartzite crust (Wet quartzite of Ranalli (1995)) represents our weakest crust end member (Fig. 2A). It is characterised by a single brittle–ductile transition that is located between 17 and 20 km depth for an average strain rate varying between 10^{-13} and 10^{-17} s^{-1}. Our layered lithospheric model is composed of a two-layer crust (Fig. 2B) in which the upper 20 km is composed of quartzite rheology and the lower part (15 km thick) of plagioclase (An_{75} of Ranalli (1995)). Two brittle–ductile transitions occur within the crust and are initially located at around 20 and 25 km, respectively. This crustal model corresponds to the one used in our previous study (Duretz et al., 2011). Our strongest crust model (Fig. 2C) consists of a single layer of granulitic rheology (felsic granulite of Ranalli (1995)). Within this crust, the brittle–ductile transition takes places at depth ranging from 20 to 30 km for corresponding strain rates of 10^{-13} and 10^{-17} s^{-1}. The Peierls mechanism is active in each of the presented lithospheric model. It takes over Mohr–Coulomb plasticity in the lithospheric mantle. The integrated strength of each lithospheric model for variable average strain rate is depicted in Fig. 2E. The quartzite crust exhibits a strength ranging from 2×10^{13} to 5×10^{13} N/m whereas the granulite crust is generally 1.25 times stronger. Although we do not notice a significant difference of integrated strength between the quartzite/plagioclase and the granulite crust, we expect that rheological layering will play an important role on the evolution of our subduction–collision models.

3.3. Mechanical decoupling between lithospheric levels

As described in the above section, our simulations employ three different crustal rheological models. The interface between the various lithospheric levels are characterised by their degree of mechanical decoupling. We here term mechanical decoupling the competence contrast that can develop between the different layers of the lithosphere (UC, LC, ML). We introduce an analysis parameter, σ^*, which expresses the effective stress ratio that can exist at the interface between two lithospheric layers. Initially, the Moho of the wet quartzite crust model is characterised by a much larger σ^* than the granulite crust model (Fig. 2A, C). The layered crust model contains two levels of moderate σ^* that are located at the upper/lower crust interface and the Moho (Fig. 2B). The granulite crust model is characterised by a moderate decoupling at the Moho. Although these quantities evolve during thermo-mechanical simulations, these horizons are likely tocontrol the localisation of deformation. We thus expect that rheological layering will strongly condition the overall evolution of our subduction–collision systems.

3.4. Potential for buoyant extrusion and crust exhumation

In order to predict wether a given crustal layer will extrude itself from the subduction zone in a buoyant flow manner, we propose a simple analysis. This process takes place as soon as a given crustal level reaches a strong buoyant stress for a relatively low flow stress. It is therefore very much controlled by the crustal rheology and the burial depth. Incidentally, this mechanism is intrinsically linked to subduction/collision dynamics since buoyant flow promotes crustal decoupling and, thus, delamination. We define ξ such as $\xi = \frac{\Delta\rho(y) g y}{\sigma_{II}}$, where $\Delta\rho(y)$ is the mean crust/mantle density contrast. Large values of ξ implies that the buoyant stress (numerator) exceeds the actual stress, potentially leading to delamination. Fig. 3A shows the magnitude of ξ as a function of depth for $\Delta\rho = 500$ kg/m^3. A wet quartzite rheology produces lower stresses than a felspar or a granulitic rheology at comparable P, T, $\dot{\epsilon}_{II}$ conditions. The corresponding ξ value can therefore reach large values (>50) and buoyant extrusion may take place.

4. Subduction–collision experiments

In this section, we describe the results of two dimensional subduction–collision numerical experiments. The experiments employ the three lithospheric models described in the above section. We

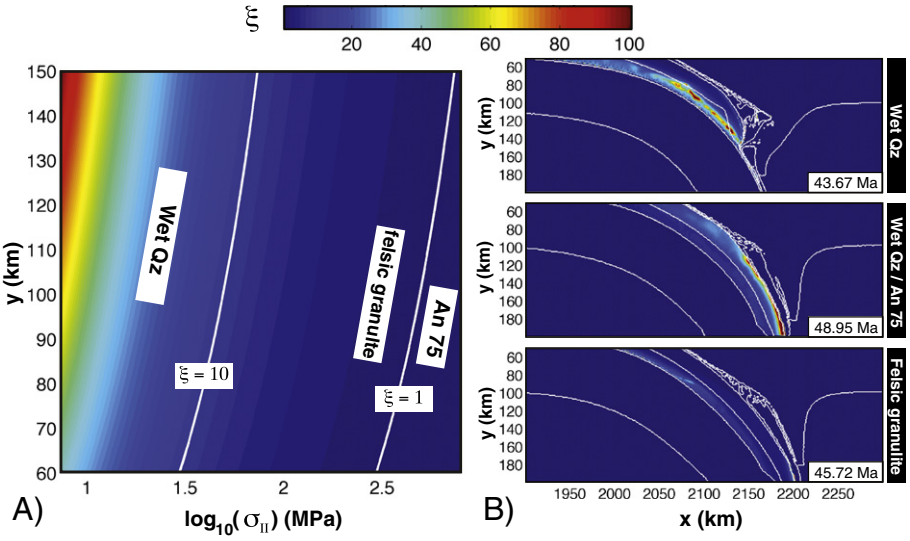

Fig. 3. Delamination potential of the crustal levels during continental subduction. The number ξ represents the ratio between the buoyancy stress induced by the crust/mantle density difference and the second stress invariant. A) The plot depicts the magnitude of ξ for variable depth and stress. The white contours indicate values $\xi = 1$, and $\xi = 10$. B) The figure panels show the magnitude of ξ for each crustal rheological model during continental subduction. The white contours represents lithological boundaries (sediments, upper crust, lower crust, mantle lithosphere, asthenosphere). The magnitude of ξ within the sediments is not shown.

focus specifically on the impact of crustal rheology on the occurrence of slab detachment, the geometry of the collision zone and the development of topography. The lithological evolution of three collision end-members are depicted in Figs. 4–6 and their respective tectonic and topographic evolutions are detailed in the following subsections.

5. Weak crust end-member: Rollback and delamination

5.1. Time evolution

The weak crust rheological model is uniquely composed of wet quartzite (see Section 2). Fig. 4 depicts the evolution of the composition field throughout the simulation. The model first undergoes kinematic compression in order to initiate an oceanic subduction zone. In spite of compression, the continental crust is sufficiently weak and suffers from extension and formation of a supra-subduction basin. This thinning event results from the viscous drag exerted by the down-going plate. After 40 Myr, the oceanic basin is closed and continental crust subduction initiates. At this stage, the simulation is mainly driven by the slab pull force, which drives the continental margin down to a maximum depth of 150 km within 3 Myr. While the crust reaches this depth, it builds up a substantial amount of positive buoyancy (~10^{13} N/m). A strong competence contrast develops between the olivine lithospheric mantle and the wet quartzite crust. The stress ratio σ^* across the Moho exceeds 50, facilitating the delamination of the mantle lithosphere (Fig. 7A). As the buoyant crust decouples from the mantle, it thickens leading to the widening of the subduction channel. Continental collision is driven by the ongoing delamination and triggers deformation of the lower plate. Crustal buckling initiates close to the suture and propagates towards the foreland following the delamination front. The wavelength of the crustal scale folds reaches ~50 km. This deformation leads to a significant thickening of the continental crust and the development of 70 km thick orogenic root overlying the asthenosphere. As the mantle lithosphere fully delaminates from the crust, there is no lasting continental margin subduction and therefore no slab detachment takes place. Since no major slab pull perturbation occurs, slab retreat and delamination freely develop and positively feedback each other. This mechanism is likely to continue as long as continental material is provided into the convergence zone.

5.2. Topographic evolution

The topographic evolution of the simulation is shown on Figs. 8A and 9A. This topographic map shows that each of the geodynamic process described in the preceding section has it own surface expression. The

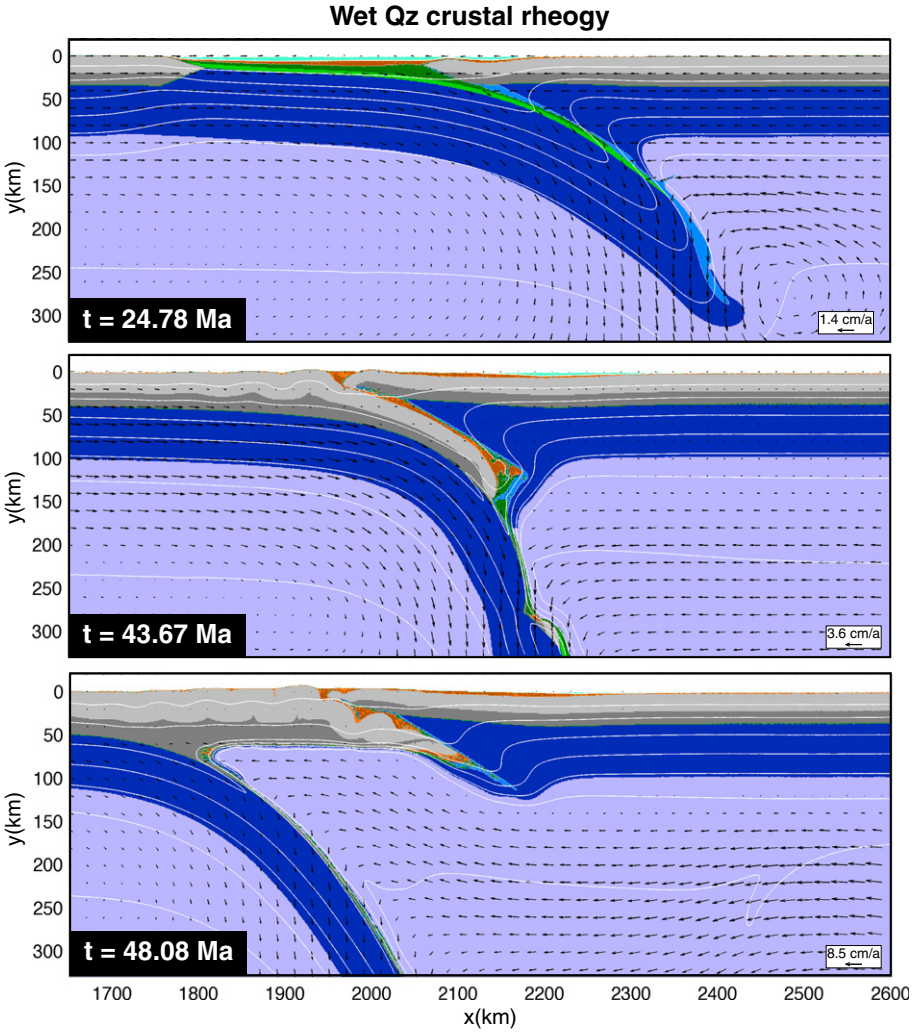

Fig. 4. Temporal evolution of the weak crust end-member. The crust is composed of a single layer of wet quartzite rheology (Ranalli, 1995). The snapshots represents the compositional field at three different periods: oceanic subduction, continental subduction and onset of delamination, plate decoupling and slab retreat. The black arrows depict the flow velocity magnitude and direction.

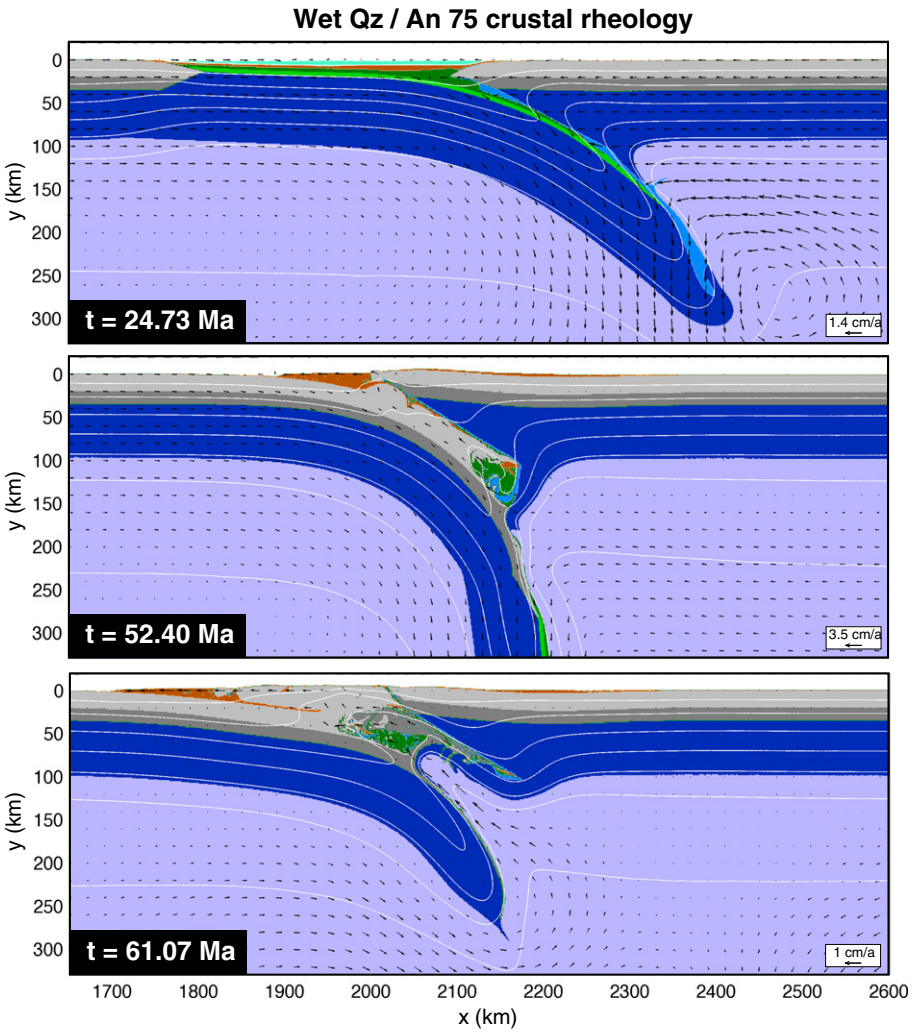

Fig. 5. Evolution of the compositional field for the layered crust model. The upper crust (20 km thick) is composed of wet quartzite and the lower crust (15 km thick) of plagioclase (An_{75}) (Ranalli, 1995). The collision system successively undergoes delamination, slab detachment and plate eduction. The flow pattern is represented by the black arrows.

first topographic feature, which is also shared with the other models (Sections 5 and 8), is the subsidence of the overriding margin during the stage of oceanic basin closure. This subsidence is triggered by the initiation of subduction and the subsequent development of slab pull. The subduction deflects the plates in the vicinity of the plate interface, coinciding with the development of the supra-subduction basin described in the above section. A deep subduction trench (~10 km) develops with ongoing subduction. Towards the end of oceanic basin closure, the continents exert compression on the accretionary prism, which leads to its exhumation and the development of the first topographic high (1–2 km). Continental subduction initiates ~1 Myr after the exhumation of the prism. The subduction of continental material causes the uplift of the overriding plate, the maximum topography is thus located in the vicinity of the plate suture. After 3 Myr of continental burial, delamination of the lower plate's mantle lithosphere commences. As the slab delaminates and sinks, it transfers compression to the overlying crust, which thickens and buckles. This crustal deformation leads to high topography areas (>2 km) coinciding with the low wavelength (~50 km) crustal antiforms. With ongoing slab retreat, the topography develops towards the foreland and reaches its peak altitude 4 Myr after the onset of delamination (i.e. 7 Myr after the onset of collision). An area of high topography is also produced on the upper plate above the suture. In this location, the crust is underthrusted by allochtonous crust, resulting in a crustal thickening.

5.3. Exhumation

In this type of model there is no major HP–UHP exhumation event. Despite the fact that the subducted continental crust has the tendency to flow towards the surface, the material becomes accumulated under the weak, thickened, orogenic root (see Fig. 10A). The exhumation of crust is driven by buoyant flow. The subducting quartzite crust has a low flow stress and cannot sustain long term subduction. Fig. 3B shows that ξ reaches 50 to 100, hence promoting buoyant extrusion. Nonetheless, the crust remains in a compressive state driven by protraction of the delaminating lithosphere. This compression inhibits the return of buried material up to the surface. The structures that are associated to the delamination are the Moho and the subduction plane which are subjected to large strain rates (Fig. 11A $t = 45.88$ Myr). On a longer timescale (~100 Myr), and in the absence of any additional tectonic event (i.e. slab detachment, Rayleigh–Taylor instabilities),we would expect the lower crust to be exhumed within the fold syntaxes driven by erosion.

6. Intermediate crustal rheology: delamination & slab detachment

6.1. Time evolution

The intermediate crustal strength model is composed of a two-layer crust (Fig. 2A), the temporal evolution of this model is described in

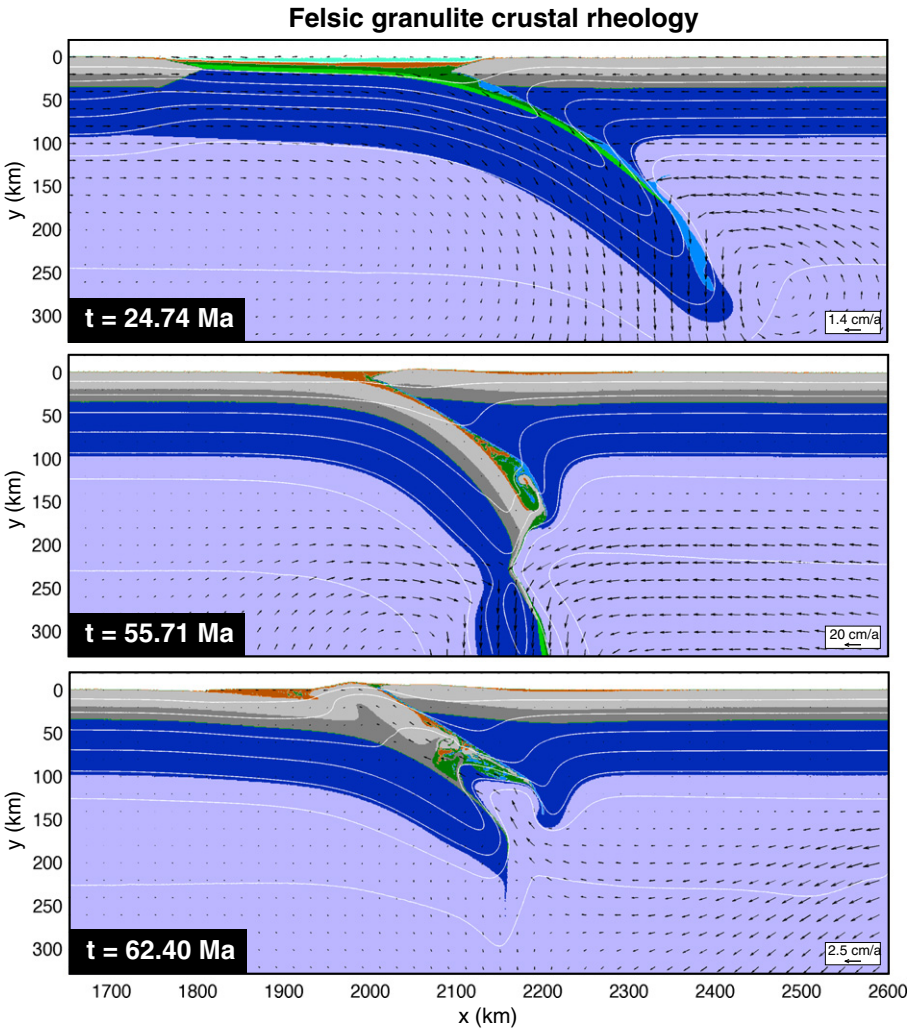

Fig. 6. Development of the collisional system for a single layered crust of felsic granulite rheology (Ranalli, 1995). The crust remains mostly undeformed during continental subduction, slab detachment occur triggering plate eduction and exhumation of a coherent crustal slice. The black arrows depict the flow velocity magnitude and direction.

Fig. 5. In contrast to the weak crust end member (Fig. 4), no extension takes place within the overriding margin during the initial stage of convergence. The stage of continental crust subduction last for ~7 Myr. When the crust reaches the burial depth of ~50 km, the stress ratio σ^* at the upper/lower crust interface exceed σ^* at the Moho (Fig. 7B). Deformation thus localises at this interface, the weaker upper crust loses its coherency and starts delaminating from the lower crust. This buoyant flow and thickening of the upper crust leads to the widening of the subduction channel. Consequently,inflow of hot mantle initiates in the deeper parts of the subduction channel and enhances plate decoupling. In contrast, the lower crust remains coupled to the mantle through the Moho. It is thus dragged down by the slab to depths of about 250 km where detachment eventually occurs, localising at the ancient ocean–continent transition. Following the loss of slab pull, the orogen undergoes a period of eduction. This mechanism is characterised by the reactivation of the subduction plane into a normal sense shear zone. The extensional stage is driven by the buoyancy of the crust, which remains coupled to the slab within the orogenic root. This mechanism is facilitated by enhanced mechanical coupling at the Moho, such as provided by this rheological structure. The subducted crustal material is exhumed towards the surface by means of both eduction and delamination-assisted flow. The extruded material spreads towards the foreland in a channel flow manner. The lower crust, which is subjected to heating in the mantle, weakens and finally decouples from the slab. The delaminated crust diapirically ascends towards the lower part of the orogenic root. At this stage, the crustal thickness gradually increases from 35 km in the foreland up to 75 km in the vicinity of the suture zone, most of the thickening is accommodated by the lower plate.

6.2. Topographic evolution

Each of the collision-related geodynamic processes described in the previous section result in strong imprints during topographic evolution (Figs. 8B, 9B). In contrast to weak crustal model (Section 2), no extension occurs in the overriding plate during convergence. Despite that fact, the upper continental margin is affected by a period subsidence which is induced by the development of slab pull beneath it. Once the two continental plates start colliding, the accretionary wedge is pinched between the two converging plates and is responsible for the location of the initial topographic high. This timespan (40–42 Myr) is marked by the initiation of continental subduction. The underthrusting of continental material under the upper plate's lithosphere leads to a long wavelength topographic bulge (~80–100 km). Positive topography develops on both sides of the plate suture despite any significant amount of crustal thickening. After ~7 Myr of continental subduction, the buried upper crust start delaminating and the subduction channel widens. This decoupling event leads to the buoyant

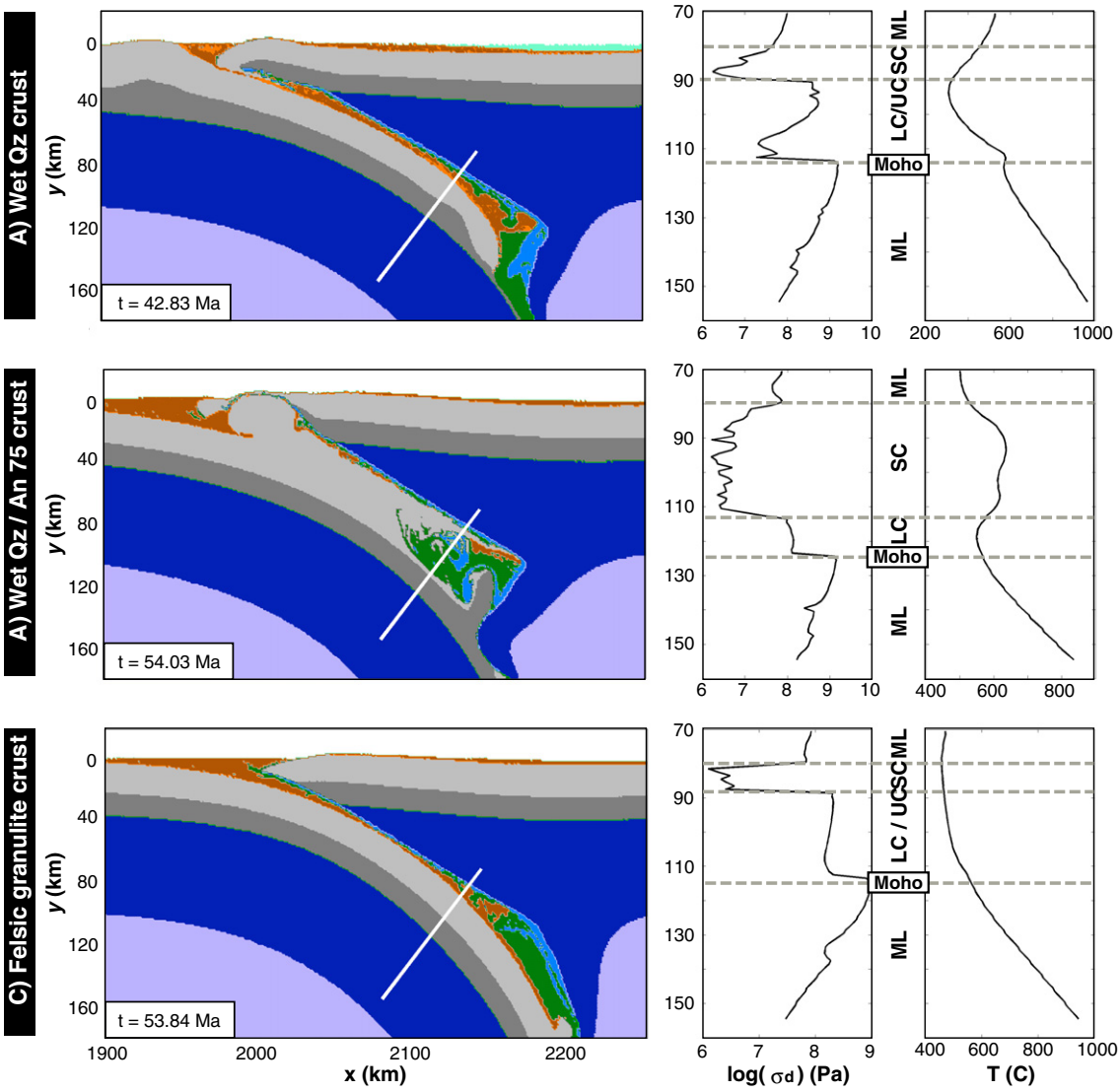

Fig. 7. Structure and rheological layering within the subduction zone at later stages of continental crust subduction for the three collisional modes. The white lines visible on the composition maps highlights the location of the differential stress and temperature profiles. The mechanical decoupling levels are indicated by the dashed grey lines. LC, UC, ML, SC respectively stands for lower crust, upper crust, mantle lithosphere and subduction channel.

extrusion of upper crust over the lower plate and has a strong topographic influence. The migration of the orogenic front towards the foreland (lower plate) coincides with slab retreat. This orogenic front migration takes place at a rate of ~2 cm/yr. After 15 Myr of collision, slab detachment takes place and triggers the sharpest topographic and surface uplift signals. As the orogen is partially decoupled prior to detachment, the topographic response of slab detachment mostly affects the lower plate and is characterised by the uplift of a 150 km wide region. This surface uplift is rapid and reaches instantaneous rates of about 10 mm/yr within a period shorter than 1 Myr. After this block uplift, the orogenic front continues migrating towards the foreland at a rate of 2–3 mm/yr. This migration is the surface expression of crustal flow, as the continental material is being extruded from the subduction channel.

6.3. Exhumation

In this simulation, several mechanisms are responsible for the exhumation of the buried crust. The first mechanism is the buoyant return flow of the crust within the subduction channel. Here the quartzite crust is weaker than the felspar lower crust and rapidly reaches high ξ (>50) (Fig. 3B). Decoupling occurs between the upper and lower crust and large strain rates develop at the interface between upper and lower crust (Fig. 11B). As a result the upper crust exhumes earlier than the lower crust and is affected by a shorter P–T history (Fig. 10B). This mechanism occurs coevally to slab retreat and yields to fast instantaneous exhumation velocities (up to 6 cm/yr). The second geodynamic event that contributes to exhumation is plate eduction consequently to slab detachment. As the lower crust remains coherent (ξ<10) and coupled to the slab. It thus subducts to greater depths until the slab detaches. After detachment, the remaining slab is characterised by continental lithosphere, which is positively buoyant. Eduction takes place and triggers the partial extraction of the slab from the mantle. The contribution of slab detachment to the exhumation is depicted on Fig. 10B. The maximum vertical velocity reaches 10 cm/yr during a short period of time (<3 Myr) in the footwall of the former subduction plane. In this model, the combination of eduction together with buoyant flow is responsible for the exhumation of the subducted continental crust. The extrusion of continental material leads to the development of crustal channel flow towards the foreland, which is visible in the strain rate field at mid-crustal depth (Fig. 11B at t = 56.33,59.07 Myr).

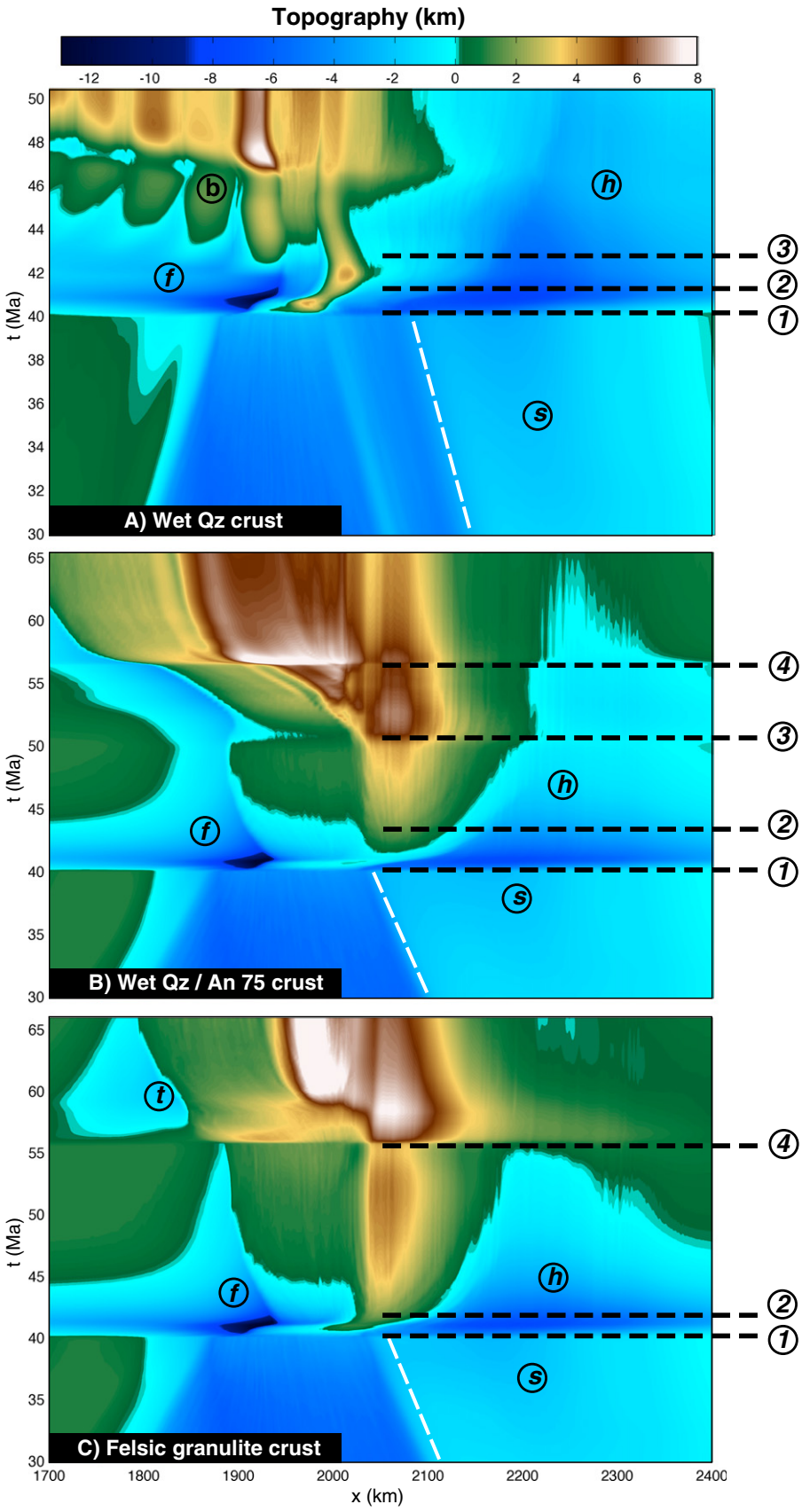

Fig. 8. Topographic evolution of the three collisional end-members. The different labels correspond to: 1) exhumation of the accretionary prism, 2) onset of continental subduction, 3) start of delamination, 4) slab detachment, s) subsidence of the upper plate, f) foreland basin, h) hinterland basin b) surface trace of crustal buckling. The white dashed line indicates the position of the trench.

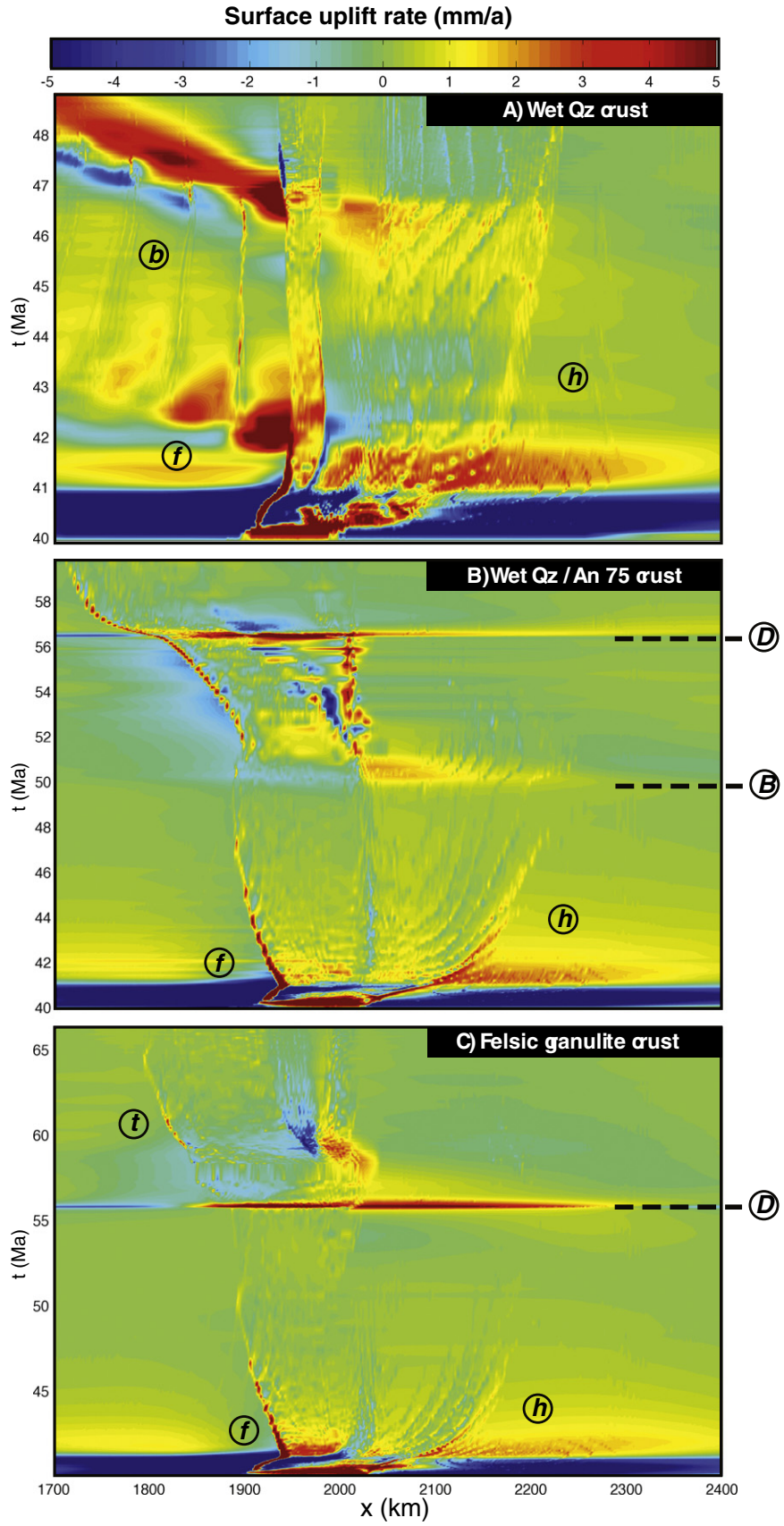

Fig. 9. Surface uplift variation during the evolution of the three collisional modes. The label D corresponds to the signal of slab detachment, B corresponds to the onset of buoyant flow. The symbols f), h) b) respectively indicates the locationof the foreland basin, the hinterland basin and the surface trace of crustal buckling.

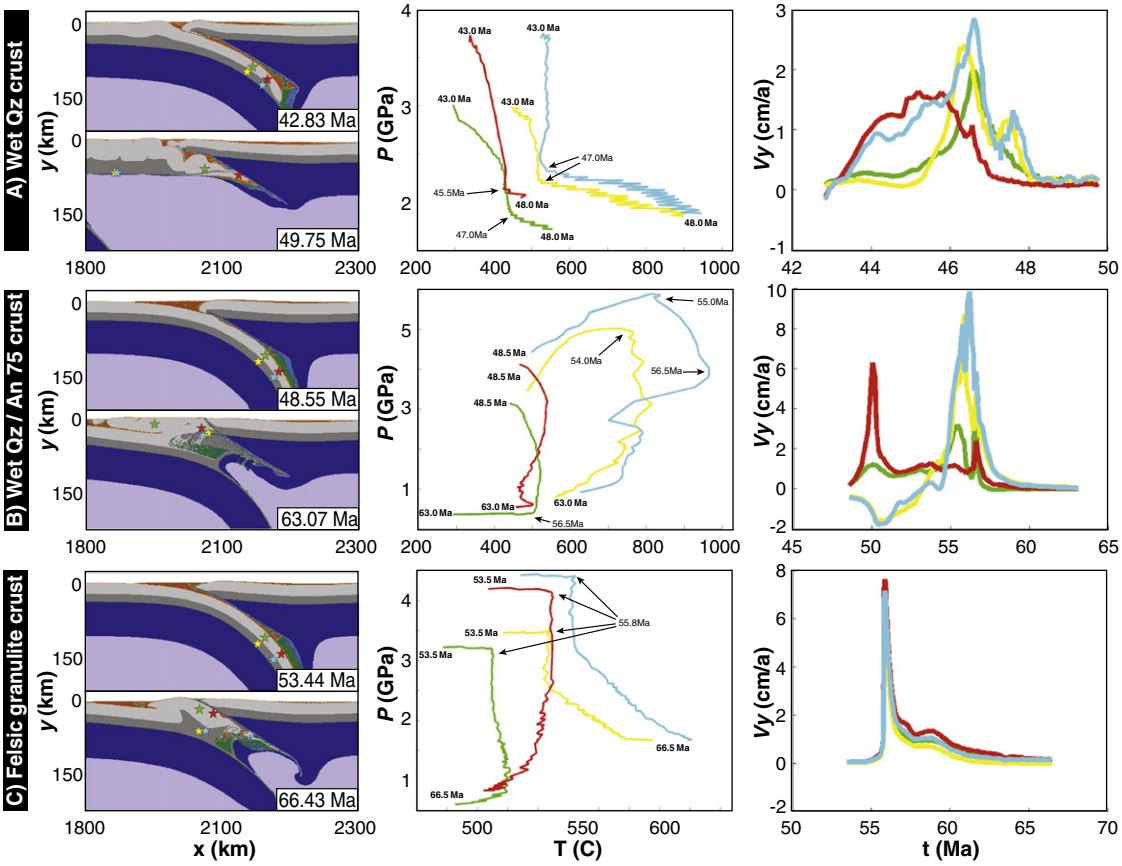

Fig. 10. The three collisional models and their contrasting styles of exhumation. The composition map is show at the left side, the coloured stars correspond to Lagrangian. The pressure–temperature paths, and vertical velocity of the corresponding Lagrangian material tracers is displayed on the graphs. The times in bold font correspond to the start/end of the P–T–t path, the times indicated with an arrow correspond to important events (buoyant flow, eduction).

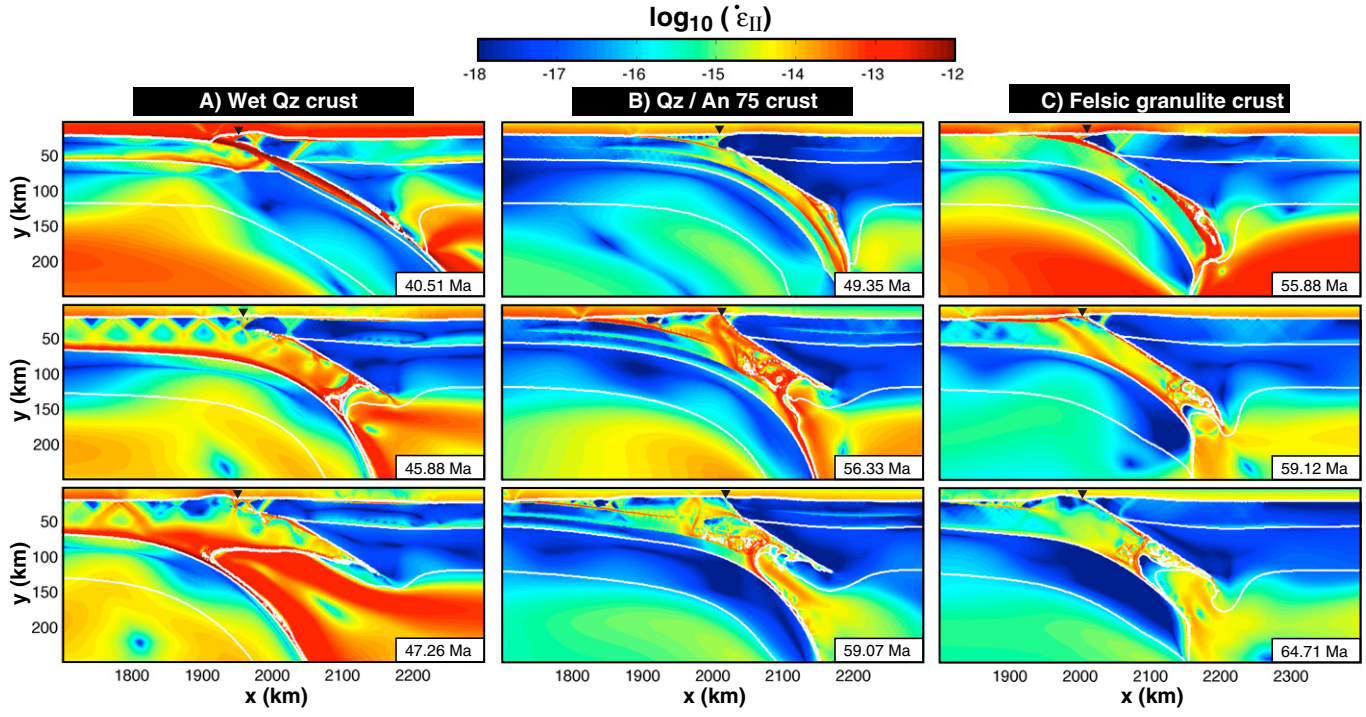

Fig. 11. Second strain rate invariant field for the three end-members (A, B, C). The time evolution of each model is depicted via three snapshots. The time is incremented from the start of the experiment. White contours lines highlight the interfaces separating the air, crust, mantle lithosphere, and asthenosphere.The black triangles indicate the position of the plate suture.

7. Strong crust end-member: slab detachment and eduction

7.1. Time evolution

The compositional cross sections depicted on Fig. 6 represent the time evolution of the strong crust model (Fig. 2C). Due to the strong nature of the crust, stresses exerted by the downgoing slab does not yield to extension in the overriding margin. After 40 Myr of oceanic subduction, continental subduction initiates and lasts during ~15 Myr. Although the crust has a similar buoyancy to that of the previous experiments, its remains coherent at depth, thanks to its strong granulitic rheology. Since the stress contrast σ^* at the Moho is minimised (<10), an episode of deep continental subduction is facilitated (Fig. 7C). The subducted margin reaches a peak burial depth (~200 km) until the crustal buoyancy balances the slab pull force. At that point, slab detachment takes place and separates the buoyant part of the slab (continental lithosphere) from the dense subducted oceanic plate. Subsequently to slab detachment, the buoyant portion of the slab is educted. The eduction stage is characterised by the coherent exhumation of the continental lithosphere (i.e. no decoupling) and the inversion of the subduction thrust into a normal-sense shear zone. After ~3 Myr of plate eduction, the crust starts deforming and decouples from the mantle lithosphere to form a slice. This crustal slice is exhumed along a basal shear zone which is rooted in the Moho of the slab and expressed as foreland dipping thrust in the crust. Throughout the exhumation, the crust is subjected to a substantial amount of thickening fostering the formation of a thick (~70 km) and narrow (~100 km) orogenic root.

7.2. Topographic evolution

Similarly to the above-presented models, it is possible to monitor the influence of the different lithospheric processes on the evolution of topography (Figs. 8C, 9C). The two-first observed signals are common features of these subduction–collision models. These signals correspond to the overriding margin subsidence during oceanic subduction and the accretionary prism exhumation prior to collision. These topographic signals are respectively linked to the downward pull of the slab and the onset of collision that exhumes the accretionary prism. During the overall period of continental subduction, the topography develops on the overriding plate in response to the underthrusting of continental crust. Slab detachment occurs after ~15 Myr of continental subduction and yields to the geologically instantaneous broadening of the orogen. This surface deformation is characterised by a strong surface uplift (~15 mm/yr) within a short duration (<0.5 Myr). Since the orogen remains mechanically coupled, the topographic rebound associated with slab detachment affects both the upper and lower plates. Eduction affects mostly the lower plates' topography and the occurrence of buoyant nappe extrusion (>57 Myr) leads to the highest topographic expression. A noticeable feature of this model is the surface trace of the nappe in the lower plate's foreland. This thrust trace remains a sharp signal over a 5 Myr timespan and witnesses the activity of a deeply rooted shear zone.

7.3. Exhumation

This model involves two main mechanisms for the exhumation of the buried crust. Each of these mechanisms are linked to the rheology of the continental crust and to the degree of mechanical decoupling that exists at the Moho. The first mechanism, namely eduction, is the direct consequence of slab detachment. Eduction is driven by the buoyancy of the crust which builds up during continental subduction. After slab detachment, this force becomes dominant and triggers the extraction of the continental lithosphere from the subduction zone. Such fashion of exhumation is efficient as long the crust remains coherently coupled to the mantle lithosphere. A strong crustal rheology promotes this behaviour since it resists to buoyantextrusion (low ξ in Fig. 3B) and no decoupling occurs between the lithospheric levels (Fig. 7C). During eduction, the deformation localises in the subduction channel, which is subjected to high effective strain rates (Fig. 11C at $t=55.88$ Myr). As the continental lithosphere suffers few deformation during exhumation, all the material tracers have resembling retrograde paths (see Fig. 10C). They are characterised by a sharp kink which determines the timing of slab detachment. Detachment is followed by a short (<2 Myr) peak of exhumation rate (≈7 cm/yr) witnessing of eduction. The second mechanism is the development of a crustal slice after 3 Myr of eduction. The initiation of the thrust requires that the buoyancy stress exerted by the exhuming material overcomes the shear strength of the foreland crust. Another interesting feature of this model is that, although the suture dips as a thrust fault, it acts as a normal-sense shear zone during the entire period of exhumation (eduction and crustal slice extrusion). These major shear zones are apparent in the second strain rate invariant field depicted in Fig. 11C (at $t=59.12$ Myr).

8. Discussion

8.1. Interplay between slab detachment and delamination

According to our simulations, the interaction between slab detachment and delamination is a plausible scenario. This interaction is intrinsically linked to the rheological structure of the lithosphere. Delamination is eager to occur in the presence of rheological layering within the subducting lithosphere (see Sections 5, 6). It is favoured by a weak crustal rheology which has a potential for buoyant extrusion (high ξ values). On the other hand, slab detachment is promoted by a strong crust (Sections 6, 7) which can remain coherent (low ξ values) and provides strong coupling at the Moho. The combination of a strong lower crust (e.g. feldspar rheology) with a weaker upper crust (e. g. wet quartzite flow law) can lead to both mechanism. Slab detachment and delamination lead to different exhumation and topographic signals (Duretz et al., 2011; Gö üş et al., 2011; Ueda et al., 2012). The occurrence of both mechanisms triggers fast exhumation rates (~10 cm/yr), polyphase exhumation (Fig. 10B) and abrupt variations in the topography (Fig. 8B).

8.2. Exhumation rates, average/instantaneous surface uplift rates, and topography

In our simulations, the exhumations rates (instantaneous vertical velocity) of deeply buried rocks are on the order of 5 to 8 cm/yr. The signal of slab detachment during exhumation is associated to eduction, which occurs in a short timespan (few Myr). The fastest exhumation events (10 cm/yr) are the results of the combination of both slab detachment and delamination. On the other hand, the instantaneous surface uplift following slab detachment can reach few mm/yr. Thus surface motions are generally one order of magnitude faster than deep exhumation rates. Similarly to exhumation rates, a peak of instantaneous surface uplift rates follows slab detachment. This uplift affects both the pro and retro sides of the orogen. It reaches extreme values (>5 mm/yr) in a geologically short timespan (< 1Myr). However, the magnitude of this uplift decreases exponentially with time (see Fig. 9C). After detachment, surface uplift rates rapidly approaches values on the order of 0.5 mm/yr during approximately 5 Myr. Slab detachment is therefore likely to affect the topography over a significant amount of time (see Fig. 8C). The rapid decrease of surface uplift yields to average surface uplift rates (over 5 Myr) on the order of 0.2 to 1 mm/yr as presented in our previous study (Duretz et al., 2011).

In our simulations, which take into account the rheology the crust and a pseudo free-surface, the topography is dynamic and evolves according to the contribution of both mantle flow and deforming crust. In our simulations, evaluating the dynamic topography in the

sense of Hager et al. (1985) or Zhong and Gurnis (1992) is not an obvious exercise. The crust is actively deforming during orogeny, hence not in local isostatic equilibrium. It is therefore difficult to remove the contribution of the deforming lithosphere to the topography. However it is evident from Figs. 4, 5 or 6 that mantle flow has a profound influence on the model's results, including the topography. For example, each of our models display a long wavelength deflection of the lithosphere after the initiation of subduction. This subsidence is induced by the downward pull of the slab and the associated mantle flow. Following this qualitative observation, our results are in accordance with the previous studies on subduction zone topography (Husson et al., 2012; Zhong and Gurnis, 1992).

8.3. Geological relevance of the models and implications

The models presented above were designed to explore the role of crustal on the dynamics continental subduction/collision. In this section, we discuss the major features of our models and their relevance to geological and geophysical observations.

8.3.1. Structural collision style

Collision styles might be qualified as coupled or decoupled (Faccenda et al., 2008). A decoupled orogenic style is associated with retreating slabs. Examples of such types of orogens may include the Apennines (Reutter et al., 1980) or the Aegean domain (Jolivet et al., 2009). In contrast, coupled collisions such as the Western Alps or the Himalayas are characterised by their compressional state of stress and the thickness of their crustal wedge (Faccenda et al., 2009). Although our models differ from those of (Faccenda et al., 2008, 2009) in terms of boundary conditions and rheological model (i.e. absence of fluid-related weakening), our results manage to reproduce both orogenic styles, which are determined by the level of mechanical coupling across the Moho.

8.3.2. Crustal rheology and the occurrence of slab detachment

In contrast to our previous study (Duretz et al., 2011), slab detachment is not a systematic feature of our models. Here, purely retreating collision takes place (Fig. 4) in presence of a weak coupling at the Moho. This promotes the delamination of the lithosphere and results in a quasi free subduction, overridden by a deformable crust. The buoyant crust resists to subduction and decouples from the slab, preventing the development of strong extensional stresses within the descending slab. Such configuration delays, or potentially inhibits, the occurrence of slab detachment. The geophysical interpretation of slab detachment in collision zones such the Alps, the Carpathians, or the Himalaya (Cloethingh et al., 2004; Lippitsch et al., 2003; Lister et al., 2008; Sperner et al., 2001) might, to some extent, reflect the presence of a subducted continental marginat depth. The occurrence of prolonged continental subduction may further suggest a strong coupling at the Moho of subducting continental lithospheres. These results are in agreement with (Burov and Yamato, 2007) that showed that a weak coupling at the Moho does not promote the formation and exhumation of high pressure rocks. More generally, (Shemenda and Grocholsky, 1992) already suggested that the coupling across the Moho should be sufficiently strong to transfer stress through the crust and trigger realistic orogenic deformation patterns.

8.3.3. Continental subduction and Ultra-High Pressure metamorphism

An important aspect of continental collision is the occurrence of continental crust subduction. Here, the maximum burial depth of the crust is controlled by two major geodynamic mechanisms: (1) the occurrence of slab detachment or (2) the onset of delamination. Our results indicate that a weak lower crust favours fast delamination at the Moho, leading to a moderate burial depth (~140 km). On the other hand, a strong lower crust provides sufficient mechanical coupling at the Moho to drag continental crust deep into the mantle (>180 km) until detachment eventually occurs. Under the assumption that HP–UHP domains are produced under near-lithostatic conditions (Burov and Yamato, 2007; Yamato et al., 2008), the existence of such domains at the surface of the Earth (Chopin, 2003; Hacker et al., 2006) may witness from a strong coupling between the mantle lithosphere and the crust during periods of continental subduction. Another consequence of continental subduction is the build up of a strong buoyancy force, which promotes eduction after slab detachment (Duretz et al., 2012a). This mechanism can partially accommodate exhumation and was proposed for the tectonic evolution Caledonian (Andersen et al., 1991; Brueckner and van Roermund, 2004; Schlindwein and Jokat, 2000) and Variscan (Schneider et al., 2006) orogens.

8.3.4. Collisions and the width of inverted oceanic basins

The models presented above also assume that gravitational forces are a dominant driver of continental collision. Thus, they apply to regions which underwent subduction of a sufficiently wide (or cold) ocean basin. This may concerns orogens with a long convergence history, such as the Himalaya (Avouac, 2003; Mattauer et al., 1999), but the setting might be different for orogens such as the Alps where the pre-collisional history is less constrained (Handy et al., 2010). If compression occurs after a limited period of rifting/drifting, a wide ocean cannot be subducted and no significant slab pull can be generated. However, as discussed, far-field and along strike forces could lead to the inversion of oceanic basins. Subsequently, the presence of extensional structures, such as documented in actual orogens (Manatschal et al., 2006, 2011), are likely to condition the orogenic geometry (Jammes and Huismans, 2012).

8.3.5. Topographic implications

Our models shows the topographic influence of slab dynamics on the evolution of topography, with emphasis on processes such as slab detachment and retreat. We showed that the average surface uplift related to slab dynamics are on the order of 0.5–1 mm/yr. Such uplift can affect regions of ~100 km length scale and persist over several Myr. This is in agreement with geological observation that stresses the role of slab dynamics in the uplift of plateaus (e. g. Central Anatolian Plateau (Schildgen et al., 2012)). Moreover, our modelled surface uplift rates compare well with estimations. Those range between 0.3 mm/yr in Borneo (Morley and Back, 2008) and 0.25–0.5 mm/yr in Central America (Rogers et al., 2002) and might be related to slab detachment.

8.4. Model limitations

One limitation of the simulations presented above is the mechanism that continental collision. Our semi-dynamic methodology contrasts with other studies that employed kinematic boundary conditions to drive collision (e. g. Burov and Yamato, 2007; Warren et al., 2008). Although this approach has the advantage to reproduce the convergence slowdown due to continental collision and dynamic consequences of slab detachment (uplift, eduction, extension), it does not allow a strong control on far-field plate kinematics. The use open sidewalls (e. g. Chertova et al., 2012; Quinquis et al., 2011) has the ability to inhibit return flow from sidewalls and can be coupled together with an applied normal stress condition (Chertova et al., 2012). This methodology is likely to better render far-field tectonic stresses without explicitly applying kinematic boundary conditions, hence, prescribing directions and rates of plate motion.

Another limitation of these model is their two-dimensional nature. Our simulations do not allow transtensional and transpressional deformation nor lateral extrusion. However, slab detachment dynamics can differ in three dimensions, exhibiting inhomogeneous dynamics in the trench direction (Burkett and Billen, 2011; van Hunen and Allen, 2011). Progressive slab detachment in the trench direction is likely to affect the style of exhumation, topography (Wortel and Spakman, 2000) and the overall plate kinematics (Austermann et al., 2011). As pointed out by Alvarez (2010), the process of continued

convergence following slab detachment remains poorly understood. In our simulations, only the delamination (weak crust) model allows to maintain a compressive stress state in the orogen. Models involving slab detachment ultimately lead to extension in response to the complete loss of slab pull. We can still expect that, if slab detachment occurs sufficiently deep (>300 km), the negative buoyancy of the hanging slab combined with far-field forces might be sufficient to maintain convergence. On the other hand, it is important to take into account three-dimensional effects such slab pull transmission (in the along-trench direction) from adjacent areas where slabs are still attached. This mechanism, which remains poorly explored, may lead to the continued convergence despite the local occurrence of slab detachment.

In this study, tectonic forces may also be a concern. Recent studies highlighted the role of mantle drag in driving plate tectonics (Alvarez, 2010; Husson, 2012). The magnitude of this force scales with the plate length and is likely to be large if the slab/asthenosphere viscosity contrast is low ($<10^2$–10^3) and the dimension of the plates is large. In combination with hot spots, drag force may lead to drastic plate accelerations (Cande and Stegman, 2011). Such force may also be responsible for maintaining long term compression in orogens that underwent slab detachment (Alvarez, 2010). Future thermo-mechanical models should thus explore the rheological conditions that would allow such force budgets together with stable convergent plate dynamics.

9. Conclusions

Our results show that the lithology of the crust, as well as its rheological structure, can by itself control the overall dynamics of subduction/collision systems. The results are supported by a simple quantification of the mechanical decoupling between the lithospheric levels (σ^*) and the potential of the crust to be subjected to buoyant extrusion (ξ). A strong crustal rheology enables mechanical coupling at the Moho (small σ^*), this configuration favours the subduction of crust. Deep continental subduction is facilitated by the strong crust that can remain coherent during burial (low ξ). Subduction may attain 200 km, depth at which slab detachment eventually takes place. Subsequently coherent exhumation of the crust is driven by means of eduction and thrusting. These orogens become bivergent subsequently to slab detachment and are characterised by a high (> 4.5 km) and narrow (<200 km) topography in the vicinity of the suture. Conversely, a weak crustal rheology provides decoupling at the Moho (high σ^*). Such promotes the delamination of the lithosphere with ongoing subduction and the extrusion of the subducting crust (high ξ). Delamination can inhibit the occurrence of slab detachment and can lead to crustal shortening driven by protraction of the overlying crust. The buckling of the crust, which is decoupled from the mantle lithosphere, triggers the development of periodic (50 km) topographic bulging locatedon the lower plate's foreland. Layered crustal models introduce an additional level of decoupling at mid-crustal depths (high σ^*). Such rheological configuration promotes the delamination of the upper crust and the deep subduction of the lower crust (small σ^* at the Moho). This type of collision can therefore be successively affected by delamination (associated to rollback) and slab detachment. The extrusion of the upper crust is fostered by buoyant flow (high ξ), which may occur during the burial of weak crust (e. g. wet quartzite rheology). The exhumed crust propagates in a channelised manner onto the foreland (lower plate) and results in the broadening of the orogen. The lateral growth of the orogen is further enhanced by the occurrence of slab detachment that affects topography on both the upper and lower plates. These results may indicate that the occurrence of both delamination (Apennines) and slab detachment (Himalayas) in orogens is strongly related to initial differences in terms of crustal rheology and structure.

Acknowledgments

Laurent Husson and an anonymous reviewer are thanked for constructively reviewing the early manuscript. Thanks to Albounet Souche and Sergeï Medvedev for providing the topographic colormaps. The manuscript benefited from discussions with Laetitia Le Pourhiet and Loic Labrousse. Author TD was funded by the SNF-EU research grant 20TO21-120535 (TOPO-4D).

References

Afonso, J., Ranalli, G., 2004. Crustal and mantle strengths in continental lithosphere: is the jelly sandwich model obsolete? Tectonophysics 394, 221–232.
Altunkaynak, Ş., Can Genç, Ş., 2004. Petrogenesis and time-progressive evolution of the Cenozoic continental volcanism in the Biga Peninsula, NW Anatolia (Turkey). Lithos 102 (1–2), 316–340.
Alvarez, W., 2010. Protracted continental collisions argue for continental plates driven by basal traction. Earth and Planetary Science Letters 296 (34), 434–442 (URL http://www.sciencedirect.com/science/article/pii/S0012821X10003481).
Andersen, T.B., Jamtveit, B., Dewey, J.F., Swensson, E., 1991. Subduction and eduction of continental crust: major mechanisms during continent–continent collision and orogenic extensional collapse, a model based on the south Norwegian Caledonides. Terra Nova 3, 303–310.
Andrews, E.R., Billen, M.I., 2009. Rheologic controls on the dynamics of slab detachment. Tectonophysics 464 (1–4), 60–69.
Austermann, J., Ben-Avraham, Z., Bird, P., Heidbach, O., Schubert, G., Stock, J.M., 2011. Quantifying the forces needed for the rapid change of Pacific plate motion at 6 Ma. Earth and Planetary Science Letters 307, 289–297.
Avouac, J.-P., 2003. Mountain building, erosion, and the seismic cycle in the nepal himalaya. Vol. 46 of Advances in Geophysics. Elsevier, pp. 1–80 (URL http://www.sciencedirect.com/science/article/pii/S0065268703460019).
Babist, J., Handy, M.R., Konrad-Schmolke, M., Hammerschmidt, K., 2006. Precollisional, multistage exhumation of subducted continental crust: The sesia zone, western alps. Tectonics 25 (6).
Baumann, C., Gerya, T.V., Connolly, J.A.D., 2009. Numerical modelling of sponaneous slab breakoff dynamics during continental collision. In: Spalla, M., Marotta, A., Gosso, G. (Eds.), Advances in interpretation of geological processes: refinement of multi-scale data and integration in numerical modelling. : Vol. 322 of Geological Society of London Special Publication. Geological Society, London, pp. 99–114.
Bird, P., 1979. Continental Delamination and The Colorado Plateau. Journal of Geophysical Research 84 (B13), 7561–7571.
Brueckner, H.K., van Roermund, H.L.M., 2004. Dunk tectonics: A multiple subduction/eduction model for the evolution of the Scandinavian Caledonides. Tectonics 23.
Buiter, S.J.H., Govers, R., Wortel, M.J.R., 2002. Two-dimensional simulation of surface deformation caused by slab detachment. Tectonophysics 354 (3–4), 192–210.
Burkett, E.R., Billen, M.I., 2011. Three-dimensionality of slab detachment due to ridge–trench collision: Laterally simultaneous boudinage versus tear propagation. Geochemistry, Geophysics, Geosystems 11.
Burov, E., Watts, A., 2006. The long-term strength of continental lithosphere:“ jelly sandwich” or “crème brulée”? GSA Today 16 (1), 4–10.
Burov, E., Yamato, P., 2007. Continental plate collision, P–T–t–z conditions and unstable vs. stable plate dynamics: Insights from thermo-mechanical modelling. Lithos 103, 178–204.
Burov, E.B., 2011. Rheology and strength of the lithosphere. Marine and Petroleum Geology 28, 1402–1443.
Cande, S.C., Stegman, D.R., 2011. Indian and African plate motions driven by the push force of the RŽunion plume head. Nature 475, 47–52.
Chatelain, J.-L., Guiller, B., Gratier, J.-P., 1993. Unfolding the subducting plate in the central New Hebrides island arc: Geometrical argument for detachment of part of the downgoing slab. Geophysical Research Letters 20 (8), 655–658.
Chen, W.P., Brudzinski, M.R., 2001. Evidence for a Large-Scale Remnant of Subducted Lithosphere Beneath Fiji. Science 292 (2575), 2475–2479.
Chertova, M.V., Geenen, T., van den Berg, A., Spakman, W., 313–326, 2012. Using open sidewalls for modelling self-consistent lithosphere subduction dynamics. Solid Earth 3 (2), 313–326 (URL http://www.solid-earth.net/3/313/2012/).
Chopin, C., 2003. Ultrahigh-pressure metamorphism: tracing continental crust into the mantle. Earth and Planetary Science Letters 212, 1–14.
Clauser, C., Huenges, E., 1995. Thermal conductivity of rocks and minerals. In: Ahrens, T.J. (Ed.), Rock Physics and Phase Relations. AGU, Washington DC, pp. 105–126 (AGU reference shelf 3).
Cloethingh, S.A.P.L., Burov, E., Matenco, L., Toussaint, G., Bertotti, G., Andriessen, P.A.M., Wortel, M.J.R., Spakman, W., 2004. Thermo-mechanical controls on the mode of continental collision in the SE Carpathians (Romania). Earth and Planetary Science Letters 218, 57–76.
Cloetingh, S., Burov, E., Matenco, L., Toussaint, G., Bertotti, G., Andriessen, P., Wortel, M., Spakman, W., 2004. Thermo-mechanical controls on the mode of continental collision in the SE Carpathians (Romania). Earth and Planetary Science Letters 218, 57–76.
Crameri, F., Schmeling, H., Golabek, G.J., Duretz, T., Orendt, R., Buiter, S.J.H., May, D.A., Kaus, B.J.P., Gerya, T.V., Tackley, P.J., 2012. A comparison of numerical surface topography calculations in geodynamic modelling: an evaluation of the Ôsticky airÕ method. Geophysical Journal International 189 (1), 38–54.

Davies, H.J., von Blanckenburg, F., 1995. Slab breakoff: A model of lithosphere detachment and its test in the magmatism and deformation of collisional orogens. Earth and Planetary Science Letters 129 (1–4), 85–102.
Duretz, T., Gerya, T.V., Kaus, B.J.P., Andersen, T.B., 2012a. Thermomechanical modeling of slab eduction. Journal of Geophysical Research 117 (B08411).
Duretz, T., Gerya, T.V., May, D.A., 2011. Numerical modelling of spontaneous slab breakoff and subsequent topographic response. Tectonophysics 502 (1–2), 244–256.
Duretz, T., Schmalholz, S.M., Gerya, T.V., 2012b. Dynamics of slab detachment. Geochemistry, Geophysics, Geosystems 13 (3), Q03020.
Evans, B., Goetze, C., 1979. Temperature variation of hardness of olivine and its implication for polycristalline yield stress. Journal of Geophysical Research 84, 5505–5524.
Faccenda, M., Gerya, T.V., Chakraborty, S., 2008. Styles of post-subduction collisional orogeny: Influence of convergence velocity, crustal rheology and radiogenic heat production. Lithos 103, 257–287.
Faccenda, M., Minelli, G., Gerya, T., 2009. Coupled and decoupled regimes of continental collision: Numerical modeling. Earth and Planetary Science Letters 278 (3–4), 337–349.
Ferrari, L., 2004. Slab detachment control on mafic volcanic pulse and mantle heterogeneity in central Mexico. Geology 32 (1), 77–80.
Gerbault, M., Willingshofer, E., 2004. Lower crust indentation or horizontal ductile flow during continental collision? Tectonophysics 387, 169–187.
Gerya, T.V., 2010. Introduction to Numerical Geodynamic Modelling. Cambridge University Press.
Gerya, T.V., Yuen, D.A., 2003a. Characteristics-based marker method with conservative finite-difference schemes for modeling geological flows with strongly variable transport properties. Physics of the Earth and Planetary Interiors 140 (4), 293–318.
Gerya, T.V., Yuen, D.A., 2003b. Rayleigh–Taylor instabilities from hydration and melting propel 'cold plumes' at subduction zones. Earth and Planetary Science Letters 212 (1–2), 47–62.
Gerya, T.V., Yuen, D.A., Maresch, W., 2004. Thermomechanical modelling of slab detachment. Earth and Planetary Science Letters 226 (1–2), 101–116.
Gö üş, O., Psyklywec, R., Corbi, F., Faccena, C., 2011. The surface tectonics of mantle lithosphere delamination following ocean lithosphere subduction: Insights from physically scaled analogue experiments. Geochemistry, Geophysics, Geosystems 12 (3), Q05004.
Hacker, B.R., McClelland, W.C., Liou, J.G., 2006. Ultrahigh-pressure metamorphism: Deep continental subduction. Vol. 403. Geological Society of America Special Papers.
Hager, B.H., Clayton, R.W., Richards, M.A., Comer, R.P., Dziewonski, A.M., 1985. Lower mantle heterogeneity, dynamic topography and the geoid. Nature 313, 541–545.
Handy, M.R., Schmid, S.M., Bousquet, R., Kissling, E., Bernoulli, D., 2010. Reconciling plate–tectonic reconstructions of alpine tethys with the geologicalgeophysical record of spreading and subduction in the alps. Earth-Science Reviews 102 (34), 121–158 (URL http://www.sciencedirect.com/science/article/pii/S0012825210000668).
Husson, L., 2012. Trench migration and upper plate strain over a convecting mantle. Physics of the Earth and Planetary Interiors 212213 (0), 32–43 (URL http://www.sciencedirect.com/science/article/pii/S0031920112001677).
Husson, L., Guillaume, B., Funiciello, F., Faccenna, C., Royden, L.H., 2012. Unraveling topography around subduction zones from laboratory models. Tectonophysics 526529, 5–15 (Modelling in Geosciences URL http://www.sciencedirect.com/science/article/pii/S0040195111003568).
Isacks, B., Molnar, P., 1969. Mantle Earthquake Mechanisms and the Sinking of the Lithosphere. Nature 223 (5211), 1121–1124.
Jackson, J., 2002. Strength of the continental lithosphere: Time to abandon the jelly sandwich? GSA Today 12, 4–9.
Jammes, S., Huismans, R.S., 2012. structural styles of mountain building: control of lithospheric theologic stratification and extensional inheritance. Journal of Geophysical Research 117 (B10), B10403.
Jolivet, L., Faccena, C., Piromallo, C., 2009. From mantle to crust: Stretching the Mediterranean. Geophysical Journal International 30 (1–2), 198–209.
Kameyama, M., Yuen, D.A., Karato, S.-I., 1999. Thermal–mechanical effects of low-temperature plasticity (the Peierls mechanism) on the deformation of viscoelastic shear zone. Earth and Planetary Science Letters 168 (1–2), 159–172.
Katayama, I., Karato, S.-I., 2008. Rheological structure and deformation of subducted slabs in the mantle transition zone: implications for mantle circulation and deep earthquakes. Physics of the Earth and Planetary Interiors 168 (3–4), 125–133.
Keskin, M., 2003. Magma generation by slab steepening and breakoff beneath subduction–accretion complex: An alternative model for collision-related volcanism in Eastern Anatolia, Turkey. Geophysical Research Letters 30 (24), 1–4.
Kundu, B., Gahalaut, V.K., 2011. Slab detachment of subducted Indo-Australian plate beneath Sunda arc, Indonesia. Journal of Earth System Science 120 (2), 193–204.
Le Pourhiet, L., Gurnis, M., Saleeby, J., 2006. Mantle instability beneath the Sierra Nevada Mountains in California and Death Valley extension. Earth and Planetary Science Letters 251 (1–2), 104–119.
Levin, V., Shapiro, N., Park, J., Ritzwoller, M., 2002. Seismic evidence for catastrophic slab loss beneath Kamchatka. Nature 418, 763–767.
Li, L., Liao, X., 2002. Slab breakoff depth: A slowdown subduction model. Geophysical Research Letters 29 (3), 1–3.
Lippitsch, R., Kissling, E., Ansorge, J., 2003. Upper mantle structure beneath the Alpine orogen from high-resolution teleseismic tomography. Journal of Geophysical Research 108 (B8).
Lister, G., Kennett, B., Richards, S., Forster, M., 2008. Boudinage of a stretching slablet implicated in earthquakes beneath the Hindu Kush. Nature 1, 196–201.
Lu, G., Kaus, B.J.P., Zhiao, L., 2011. Thermal localization as a potential mechanism to rift cratons. Physics of the Earth and Planetary Interiors 186, 125–137.
Macera, P., Gasperini, D., Ranalli, G., Mahatsente, R., 2008. Slab detachment and mantle plume upwelling in subduction zones: An example from the Italian South-Eastern Alps. Journal of Geodynamics 45 (1), 32–48.
Manatschal, G., Engstrm, A., Desmurs, L., Schaltegger, U., Cosca, M., Müntener, O., Bernoulli, D., 2006. What is the tectono-metamorphic evolution of continental break-up: The example of the Tasna Ocean Continent Transition. Journal of Structural Geology 28 (10), 1849–1869 (URL http://www.sciencedirect.com/science/article/pii/S0191814106001726).
Manatschal, G., Sauter, D., Karpoff, A.M., Masini, E., Mohn, G., Lagabrielle, Y., 2011. The chenaillet ophiolite in the french/italian alps: An ancient analogue for an oceanic core complex? Lithos 124 (34), 169–184 (Alpine Ophiolites and Modern Analogues. Continental Rifting to Oceanic Lithosphere. Alpine Ophiolites and Modern Analogues. URL http://www.sciencedirect.com/science/article/pii/S0024493710003002).
Mareschal, J.C., 1994. Thermal regime and post-orogenic extension in collision belts. Tectonophysics 238, 471–484.
Martin, M., Wenzel, F., 2006. High-resolution teleseismic body wave tomography beneath SE-Romania - II. Imaging of a slab detachment scenario. Geophysical Journal International 164 (3), 579–595.
Mattauer, M., Matte, P., Olivet, J.-L., 1999. A 3D model of the India–Asia collision at plate scale. Comptes Rendus de l'Acadmie des Sciences — Series IIA — Earth and Planetary Science 328 (8), 499–508 (URL http://www.sciencedirect.com/science/article/pii/S125180509980130X).
Mei, S., Suzuki, A.N., Kohlstedt, D.L., Dixon, N.A., Durham, W.B., 2011. Experimental constraints on the strength of the lithospheric mantle. Journal of Geophysical Research 115 (B08204).
Morley, C.K., Back, S., 2008. Estimating hinterlang uplift exhumation from late orogenic basin volume, NW Borneo. Journal of the Geological Society 165, 353–366.
Mugnier, J.-L., Huyghe, P., 2006. Ganges basin geometry records a pre-15 Ma isostatic rebound of Himalaya. Geology 34 (6), 445–448.
Nakada, M., 1994. Convective coupling between ductile lower crust and upper mantle, and its tectonic implications. Geophysical Journal International 118, 569–603.
Qin, J., Lao, S., Li, Y., 2008. Slab Breakoff model for the Triassic Post-Collisional Adakitic Granitoids in the Qinling Orogen, Central China: Zircon U–Pb Ages, Geochemistry, and Sr–Nd–Pb Isotopic Constraints. International Geology Review 50, 1080–1104.
Quinquis, M.E., Buiter, S.J., Ellis, S., 2011. The role of boundary conditions in numerical models of subduction zone dynamics. Tectonophysics 497 (14), 57–70 (URL http://www.sciencedirect.com/science/article/pii/S0040195110004750).
Ranalli, G., 1995. Rheology of the Earth, 2nd ed. Chapman & Hall, London.
Ranalli, G., 2000. Rheology of the crust and its role in tectonic reactivation. Journal of Geodynamics 30 (1–2), 3–15.
Raterron, P., Wu, Y., Weidner, D.J., Chen, J., 2004. Low-temperature olivine rheology at high pressure. Physics of the Earth and Planetary Interiors 145, 149–159.
Regard, V., Faccenna, C., Bellier, O., Martinod, J., 2008. Laboratory experimemts of slab break-off and slab dip reversal: insight into the Alpine Oligocene reorganization. Terra Nova 20 (4), 267–273.
Replumaz, A., Negredo, A.M., Guillot, S., Villasenor, A., 2010. Multiple episodes of continental subduction during India/Asia convergence: Insight from seismic tomography and tectonic reconstruction. Tectonophysics 483 (1–2), 125–134.
Reutter, K., Giese, P., Closs, H., 1980. Lithospheric split in the descending plate: observations from the Northern Apennines. Tectonophysics 64 (1–2), T1–T9.
Rogers, R.D., Karason, H., van der Hilst, R.D., 2002. Epeirogenic uplift above a detached slab in northern Central America. Geology 30, 1031–1034.
Schildgen, T.F., Cosentino, D., Caruso, A., Buchwalt, R., Yildirim, C., Bowring, S.A., Rojay, B., Echtler, H., Strecker, M.R., 2012. Surface expression of eastern Mediterranean slab dynamics: Neogene topographic and structural evolution of the southwest margin of the Central Anatolian Plateau, Turkey. Tectonics 31 (TC2005) (21 pp.).
Schlindwein, V., Jokat, W., 2000. Post-collisional extension of the East Greenland Caledonides: a geophysical perspective. Geophysical Journal International 140, 559–567.
Schmalholz, S.M., 2011. A simple analytical solution for slab detachment. Earth and Planetary Science Letters 304 (1–2), 45–54.
Schmalholz, S.M., Kaus, B.J., Burg, J.-P., 2009. Stress–strength relationship in the lithosphere during continental collision. Geology 332 (9), 775–778.
Schmandt, B., Humphreys, E., 2011. Complex subduction and small-scale convection revealed by body-wave tomography of the western United States upper mantle. Earth and Planetary Science Letters 297, 435–445.
Schmeling, H., Babeyko, A.Y., Enns, A., Faccenna, C., Funiciello, F., Gerya, T.V., Golabek, G.J., Grigull, S., Kaus, B.J.P., Morra, G., Schmalholz, S.M., van Hunen, J., 2008. A benchmark comparison of spontaneous subduction models — Towards a free surface. Physics of the Earth and Planetary Interiors 171 (1–4), 198–223.
Schneider, D.A., Zahniser, S.J., Glascock, J.M., Gordon, S.M., Manecki, M., 2006. Thermochronology of the West Sudetes (Bohemian Massif): Rapid and repeated eduction in the Eastern Variscides, Poland and Czech Republic. American Journal of Science 306, 846–873.
Shemenda, A.I., Grocholsky, A.L., 1992. Physical modelling of lithosphere subduction in collision zones. Tectonophysics 216, 273–290.
Sinclair, H.D., 1997. Flysch to molasse transition in peripheral foreland basins: The role of the passive margin versus slab breakoff. Geology 25, 1123–1126.
Sperner, B., Lorenz, F., Bonjer, K., Hettel, S., Müller, B., Wenzel, F., 2001. Slab break-off — abrupt cut or gradual detachment? New insights from the Vrancea Region (SE Carpathians, Romania). Terra Nova 13 (3), 172–173.
Thompson, A., Schulmann, K., Jezek, J., Tolar, V., 2001. Thermally softened continental extensional zones (arcs and rifts) as precursors to thickened orogenic belts. Tectonophysics 332 (1–2), 115–141.
Ton, S.W.A., Wortel, M., 1997. Slab detachment in continental collision zones: An analysis of controlling parameters. Geophysical Research Letters 24 (16), 2095–2098.
Toussaint, G., Burov, E., Jolivet, L., 2004. Continental plate collision: Unstable vs. stable slab dynamics. Geology 32 (1), 33–36.
Turcotte, D.L., Schubert, G., 1982. Geodynamics: Application of Continuum Physics to Geological Problems. John Wiley, New York.

Ueda, K., Gerya, T.V., Burg, J.-P., 2012. Delamination in collisional orogens: Thermomechanical modeling. Journal of Geophysical Research 117 (B08202).
vam Heck, H., Tackley, P.J., 2008. Planforms of self-consistently generated plates in 3d spherical geometry. Geophysical Research Letters 35 (L19312) (6 pp.).
van de Zedde, D.M.A., Wortel, M.J.R., 2001. Shallow slab detachment as a transient source of heat at midlithospheric depths. Tectonics 20 (6), 868–882.
van der Meer, D., Spakman, W., van Hinsbergen, D., Amaru, M.L., Torsvik, T.H., 2010. Towards absolute plate motions constrained by lower-mantle slab remnants. Nature Geoscience 3, 36–40.
van Hunen, J., Allen, M.B., 2011. Continental collision and slab break-off: A comparison of 3-D numerical models with observations. Earth and Planetary Science Letters 302 (1–2), 27–37.
Warren, C., Beaumont, C., Jamieson, R., 2008. Modelling tectonic styles and ultra-high pressure (UHP) rock exhumation during the transition from oceanic subduction to continental collision. Earth and Planetary Science Letters 267, 129–245.
Widiyantoro, S., van der Hilst, R., 1996. Structure and evolution of lithospheric slab beneath the Sunda Arc, Indonesia. Science 271, 1566–1570.
Wilmsen, M., Fürsich, F., Seyed-Emmani, K., Majidifard, M.R., Taheri, J., 2009. The Cimmerian Orogeny in northern Iran/tectono-stratigraphic evidence in the foreland. Terra Nova 21 (3), 211–218.
Wortel, M.J.R., Spakman, W., 1992. Structure and dynamics of subducted lithosphere in the Mediterranean region. Proceedings of the Koninklijke Nederlandse Akademie van Wetenschappen-Biological Chemical Geological Physical and Medical Sciences 95 (3), 325–347.
Wortel, M.J.R., Spakman, W., 2000. Subduction and slab detachment in the Mediterranean–Carpathian Region. Science 290 (5498), 1910–1917.
Xu, W.-C., Zhang, H.-F., Parrish, R., Harris, N., Guo, L., Yuan, H.-L., 2010. Timing of granulite-facies metamorphism in the eastern Himalayan syntaxis and its tectonic implications. Geology 485 (1–4), 231–244.
Yamato, P., Agard, P., Burov, E., Le Pourhiet, L., Jolivet, L., Tiberi, C., 2008. Burial and exhumation in a subduction wedge: Mutual constraints from thermomechanical modeling and natural P–T–t data (Schistes Lustrés, western Alps). Journal of Geophysical Research 112, B07410.
Zeck, H.P., 1996. Betic–Rif orogeny: Subduction of Mesozoic Tethys lithosphere under eastward drifting Iberia, slab detachment shortly before 22 Ma, and subsequent uplift and extensional tectonics. Tectonophysics 254 (1–2), 1–16.
Zhong, S., Gurnis, M., 1992. Viscous flow model of a subduction zone with a faulted lithosphere: Long and short wavelength topography, gravity and geoid. Geophysical Research Letters 19 (18), 1981.
Zor, E., 2008. Tomographic evidence of slab detachment beneath eastern turkey and the caucasus. Geophysical Journal International 175 (3), 1273–1282.